# Chapter 7
# Hybrid Polymers for Conventional and Additive Manufacturing of Microoptical Elements

**Martin Herder, Jan Jasper Klein, Marko Vogler, Maria-Melanie Russew, Arne Schleunitz, and Gabi Grützner**

**Abstract** Hybrid polymers constitute a class of optical materials combining properties of inorganic glass and organic polymers. The flexible synthesis and processing allows for specific tailoring of their properties as required for the fabrication of high-performance and reliable microoptical elements. While wafer-scale fabrication of microoptics using hybrid polymers is widely used in an industrial environment, they gain ever-increasing attention in additive manufacturing and 3D printing technologies. This chapter introduces the chemical concepts behind hybrid polymers, discusses their synthesis and processing, and gives a record on their application for the fabrication of microoptical and photonic elements using established wafer-scale as well as emerging additive manufacturing processes, in particular inkjet printing and two-photon polymerization direct laser writing.

**Keywords** Optical polymers · Microoptics · Hybrid polymers · ORMOCERs Photolithography · UV molding · Nanoimprint lithography · Additive manufacturing · Inkjet printing · 3D printing · Two-photon polymerization

## 7.1 Introduction

Microoptical elements constitute a key enabling technology for consumer electronics, telecommunication, sensing, imaging, lighting, as well as virtual and augmented reality applications [1–5]. Their sophisticated design, miniaturization, and integration are crucial for the realization of new devices with high functional complexity and energy efficiency. Current wafer-scale production technology allows for mass fabrication of microoptical elements such as microlens arrays, gratings, diffractive

M. Herder (✉) · J. J. Klein · M. Vogler · M.-M. Russew · A. Schleunitz · G. Grützner
micro resist technology GmbH, Berlin, Germany
e-mail: m.herder@microresist.de; j.klein@microresist.de



A. Heinrich (ed.), *3D Printing of Optical Components*, Springer Series in Optical Sciences 233, https://doi.org/10.1007/978-3-030-58960-8_7

optical elements (DOEs), or waveguides, as well as their integration into complex optoelectronic devices [6].

Modern 3D printing methods bring unprecedented opportunities to the fabrication of microoptics [7]: straightforward fabrication of freeform and true 3D microoptical elements as well as rapid prototyping with turnover times from the optical design to the fabricated part in the range of minutes to few hours will allow for completely new concepts in design and optimization. Furthermore, fabrication of integrated devices is simplified by direct printing onto sensors, emitters, or optical fibers.

Importantly, the rise of 3D printing as new fabrication technology goes hand in hand with the development of innovative optical materials with superior performance and processability. While a large number of conventional optical materials such as inorganic glass or organic polymers exist, their applicability in 3D printing requires adaptation or is very challenging as in the case of optical glass [8–10]. Furthermore, from a commercial viewpoint, materials must fulfill stringent quality requirements regarding not only optical performance but also environmental and long-term stability, processability, as well as cost-effectiveness.

In this respect, inorganic-organic hybrid polymers constitute a material platform showing unique properties and superior performance [11–13]. They are established commercial materials for the wafer-scale fabrication of microoptics and hold great promise for applications realized with additive manufacturing. In this review, we will point out the advantages of hybrid polymers in the context of optical materials. An introduction into synthetic routes and properties of hybrid polymers is given, and finally their application in the fabrication of microoptical components by wafer-scale and additive manufacturing technologies will be discussed.

## 7.2 Optical Materials and Fabrication Processes

### *7.2.1 Glass and Polymers for Optical Applications*

The most important material parameter for the fabrication of optical elements is the ability to reflect, refract, or diffract light while being transparent at the wavelength of interest. In addition, refractive index, dispersion, and birefringence are crucial for the design and performance of optical elements. The transparency of any material is determined by several factors: (1) For transparency in the near-UV (NUV) and visible range, the electronic band gap of the material, i.e., the energy required for the excitation of electrons, must be higher than the light energy. (2) At infrared (IR) wavelengths, transparency strongly depends on the frequency and type of atomic and molecular vibrations. (3) The size of individual structural features of the material, i.e., grain boundaries and defects, must be smaller than the wavelength of light to avoid loss by scattering.

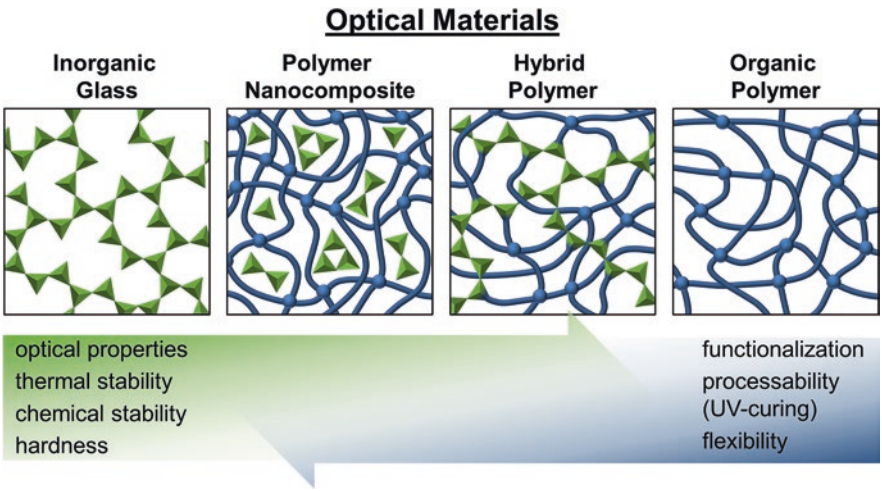


**Fig. 7.1** Architecture and properties of inorganic and organic units combined in optical materials

In this respect, historically inorganic glass is the material of choice for the fabrication of optics. Its valence electrons have no energy level available that can be reached by absorption of a visible photon, its transparency ranges to near-IR (NIR) wavelengths, and its structure is highly amorphous showing no long-range order (Fig. 7.1 left). Other inorganic ceramic and semiconducting materials applied in optics, e.g., chalcogenide glasses, silicon, silicon carbide, GaAs, or InP, generally have lower band gaps than silica glass. Thus, they are not necessarily transparent in the visible range, but show other distinct properties, e.g., increased refractive index or transparency in the IR range [3]. On the other hand, an ever-increasing number of optical quality polymers exist, which possess highly amorphous (Fig. 7.1 right) or semicrystalline structures and consist of molecular building blocks with high band gap. Typical representatives are silicones (e.g., PDMS), poly(methyl methacrylate) (PMMA), polystyrene (PS), polycarbonate (PC), acrylonitrile butadiene styrene (ABS), or cyclic olefin (co)polymer (COC/COP).

Notably, inorganic glass and organic polymers are complementary in their properties (Fig. 7.1): most glasses show maximum transparency over a wide range of wavelengths from the NUV over visible to NIR wavelengths. In addition, they are available with a wide range of refractive indices and dispersion while generally showing low birefringence [14]. In comparison, transparency of polymers is reduced, in particular in the UV range, due to absorption of specific functional groups in the backbone and increased scattering effects. The range of refractive indices and dispersion properties is much smaller than that of glass [15]. While most optical polymers are naturally isotropic, their processing often induces marked birefringence due to orientation of the polymer chains [16].

Regarding mechanical properties, differences are even more pronounced. Glasses are generally hard and brittle materials with superior chemical inertness and

stability against thermal and light damage. In contrast, the mechanical properties of polymers can be tuned over an extremely broad range from soft and flexible to hard and tough by changing their molecular architecture. In addition, organic chemistry allows for application-specific tailoring of bulk and surface properties such as gas permeability and hydrophilicity. However, due to the organic nature of the building blocks, the inertness and stability of polymers is lower compared to inorganic glass.

Importantly, these material properties dictate the choice of processes for the fabrication of optical components. Glass components in the macro- to microscale are fabricated using subtractive methods, i.e., cutting, grinding, turning, and polishing processes. Molding techniques—offering a highly parallel and cost-effective way for mass production—are limited to specific glass types possessing low $T_g$ [14]. In contrast, utilizing polymers allows for a large range of processing conditions and thus much larger freedom in the design of optical components. They are mass fabricated from thermoplastic polymers, i.e., polymers that can be melted by heating, using hot embossing or injection molding [17]. Alternatively, UV curing, i.e., light-induced polymerization and cross-linking of resins containing acrylate, epoxide, or thiol-ene functions, is advantageously used for structuring polymer layers by spatial UV exposure through a photomask (UV lithography) or pressing a stamp into the material prior to UV flood exposure and separation (UV imprinting). In particular, with thermal or UV nanoimprint lithography (NIL), optical components with micro- and nanoscale resolution can be realized using wafer-scale and roll-to-roll fabrication [18, 19]. During these processes, either the structured polymer itself becomes integral part of the optical component, or it is used as resist for transferring the structure into the underlying glass or semiconductor substrate by an etching step.

In general, due to their more facile and versatile processing, polymers are the material of choice for most 3D printing processes [20]. On the one hand, thermoplastics are employed in fused deposition modeling (FDM) and selective laser sintering (SLS), whereby these non-cross-linked polymers are heated above their glass transition temperature $T_g$ becoming liquid and being extruded or molten into the desired architecture. On the other hand, light-based 3D printing methods such as UV-assisted inkjet printing, stereolithography (SLA), or two-photon polymerization direct laser writing (2PP-DLW) rely on photocurable thermosets. Using these, maximum resolution, being of tremendous importance in the context of microoptics, is achieved due to localized curing with the high spatial and temporal resolution inherent to the application of light. In contrast to polymers, direct 3D structuring or printing of glass materials requires much harsher conditions or can only be achieved using sophisticated chemistry [8–10].

### *7.2.2 Hybrid Materials*

Regarding the complementary properties of glass and polymers, it is tempting to combine both into a unique material and profit from the advantages of both worlds. This is achieved with so-called hybrid materials [21, 22], which can be divided into class I hybrids, e.g., polymer nanocomposites, and class II hybrids, e.g., hybrid

polymers (Fig. 7.1 middle). In polymer nanocomposites clusters or particles of an inorganic material are dispersed in a polymeric matrix, and only weak interactions, such as van der Waals interactions or hydrogen bonds, exist between the two domains. In contrast, in hybrid polymers the inorganic and organic domains are grafted together by strong covalent interactions. Thus, the inorganic domain forms clusters or an extended network interpenetrating with the organic polymer. In order to be suited for applications in optics, the length scale of the individual domains should be smaller than the wavelength of light, i.e., usually in the range of few tens of nanometers, to avoid scattering effects.

Hybrid materials do not only combine the properties of the individual components, but new properties may emerge due to the nanometer length scale and resulting large interface between the inorganic and organic domain. Thus, they show an extraordinarily high mechanical, thermal, and chemical resistance as compared to bare organic polymers. At the same time, their mechanical properties are tunable showing greater flexibility and toughness compared to inorganic glass. The combination of sol-gel synthesis (*vide infra*) and polymer chemistry in hybrid materials open up new and versatile ways of material fabrication and processing. Most importantly, optical properties of hybrid materials such as refractive index and dispersion can be tuned by varying the composition of inorganic and organic domains exceeding the range offered by conventional polymers [23].

Consequently, it turns out that for applications in microoptics and photonics with high demands for optical quality, stability, and processing, high-performing hybrid materials are the optimal choice. However, for application in a commercial environment, further considerations have to be made: synthesis of a material should be scalable and cost-effective, and it should possess a shelf life of several months to years. In this respect, hybrid polymers clearly outperform polymer nanocomposites. The latter often suffer from aging and aggregation phenomena during synthesis and storage. Furthermore, stringent quality control during every stage of the production process is essential, in particular for applications in optics, to gain full control over material properties and guarantee reproducible specifications and reliable performance.

In this realm, hybrid polymers based on the ORMOCER® (ORganically MOdified CERamics) technology [24] being commercialized by *micro resist technology GmbH* under the names OrmoComp®, OrmoClear®, OrmoClear®FX, and OrmoStamp® [25] enjoy a tremendous popularity for the fabrication of microoptical components and are used worldwide in industry and academia.

### *7.2.3 Production and Processing of Hybrid Polymers*

The ORMOCER technology initially developed by the *Fraunhofer Institute for Silicate Research* is based on the sol-gel processing of organically modified alkoxides as hybrid molecular precursors. These alkoxides are mainly based on silicon, but also other metal alkoxides (e.g., Al, Ti, Zr) may be added. The resulting material consists of domains of inorganic oxidic glass (silica network), organically modified

polysiloxanes, and cross-linked organic polymers. As the covalent silicon–carbon bond is stable against hydrolysis, a permanent and strong connection between the inorganic and organic domains of the hybrid polymer is obtained. Starting from the mid-1980s, the basic chemistry and processing of ORMOCER-based hybrid polymers have been developed [26–35] leading to today's numerous applications not only in the field of optics but also as coatings, dental fillings, membranes, microelectronics, and energy conversion [21, 30].

The fabrication of hybrid polymers proceeds in three main steps (Fig. 7.2):

1. Sol-gel synthesis of the inorganic domain resulting in a solvent-free base resin.
2. Formulation by addition of comonomers, photoinitiator, and functional additives.
3. UV curing of the organic domain during processing. In the following brief details on each of the three steps are given with emphasis on how distinct choice of chemical entities or parameters influences the properties of the final hybrid polymer.

### 7.2.3.1 Sol-Gel Synthesis of the Base Resin

Sol-gel synthesis [36, 37] relies on the subsequent hydrolysis and condensation of silicon alkoxides $R'_xSi(OR)_{4-x}$ with R′ being an optional organic residue and OR a simple alcohol. In a first step, Si–OR bonds are hydrolyzed by the attack of water, and in a second step, Si–O–Si bonds are formed by condensation of silanol groups (Fig. 7.2). The condensation step is irreversible, thus with ongoing reaction time,

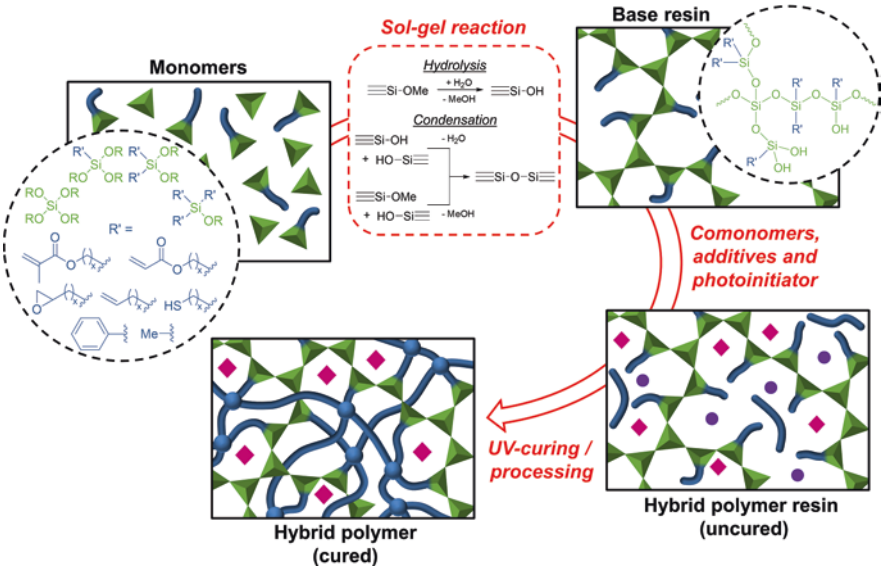


**Fig. 7.2** Synthesis and processing of hybrid polymers in three steps. Exemplary structures of silane precursors as well as possible structural motifs of the inorganic domain are shown in the insets

small, soluble particles evolve (the sol), which start to interconnect and aggregate to larger clusters finally forming an extended three-dimensional network inducing gelation of the material. Notably, during the sol-gel synthesis, the reaction is precisely controlled in order to stop it just before gelation. Thus, liquid base resins with tunable viscosities are obtained, which are easily processable by means of micro- and nanofabrication in later steps (*vide infra*). Importantly, the type of silane precursor and reaction conditions (solvent, catalysts, temperature, pH) determine the relative rates of hydrolysis and condensation. This allows for control over the Si–OH content of the resin and the size of inorganic particles, which are typically in the range of 1–3 nm [35, 38] ensuring high optical quality of the material and allowing for its structuring with nanometer resolution.

A huge variety of silane precursors $R'_xSi(OR)_{4-x}$ for the sol-gel reaction is available. Some examples are depicted in Fig. 7.2. Importantly, the number of organic residues R′ on the precursor dictates the structure of the resulting inorganic network ranging from extended 3D structures over silsesquioxane clusters and linear chains to short oligomers. Residues R′ either can be inert (e.g., alkyl or phenyl groups) or possess polymerizable functions such as acrylate, methacrylate, epoxy, vinyl, thiol, or amine groups. Size and number of organic groups again influence the network density of the inorganic domain by steric interactions, while the amount and type of polymerizable groups determine the structure of the organic network after curing. Their main task is to counteract the brittle nature of the inorganic glass-like domain and induce toughness or a certain degree of flexibility to the material after UV curing.

Usually at the end of the sol-gel reaction, base resins are dried, all solvents are removed, and the material is fine-filtered to ensure reproducible quality and tight specifications.

#### 7.2.3.2 Formulation

After sol-gel synthesis of the base resin, its properties and processability are fine-tuned by using different additives: organic comonomers as well as chain transfer agents fine-tune the structure of the organic network and optimize the curing chemistry. Furthermore, comonomers are also used to tune viscosity of the uncured resin as well as mechanical and surface properties of the cured hybrid polymer. Sol-gel additives, i.e., unreacted organoalkoxysilanes, optimize processing, in particular as adhesion promoter for coatings, thin films, and wafer-scale fabrication processes.

The choice of the photoinitiator is of particular importance for light-induced curing of the organic network. Depending on the polymerization chemistry utilized (epoxy-, vinyl- or acrylate-based systems), a large variety of photoacid generators or radical photoinitiators is available [39]. Critical parameters are optimal photosensitivity at the curing wavelength, high reactivity, low sensitivity towards oxygen inhibition, as well as nontoxicity of photoproducts. In addition, for the fabrication of optical components, full bleaching of the initiator as well as minimization of discoloration and luminescence caused by photoproducts is essential and requires careful optimization of the initiation system. In this respect, phosphine oxides (e.g., TPO) and α-hydroxy ketones show superior performance.

Further additives may include polymerization stabilizers to ensure high shelf life of the uncured hybrid polymer resins, thermo- and UV stabilizers for improving long-term stability of final products, dyes for modification of optical properties, as well as surfactants to modify surface tension and coating behavior of the resins.

#### 7.2.3.3 Processing and UV Curing

Uncured hybrid polymers being solvent-free viscous liquids can easily be processed using standard wafer-scale fabrication techniques, such as UV lithography, UV molding, nanoimprint lithography, and direct laser writing. Exemplary processing for UV lithography and UV imprinting, typically employed for the fabrication of microoptical components, is shown in Fig. 7.3 [11]. Generally, hybrid polymers behave as a typical negative-tone resist. After spin coating or dispensing of the resin, UV curing is induced under a mask in proximity exposure or while pressing a structured stamp into the material. Post-exposure bake, development and hardbake steps follow. Cross-linking of the organic domain is completed during UV curing, while the optional thermal annealing steps increase adhesion to the substrate, stabilize optical properties of the material, and further increase its thermal and environmental stability due to relief of residual internal stress.

Critical parameters during processing are the irradiation setup, $O_2$ sensitivity, and shrinkage of the hybrid polymer during curing. Hybrid polymers are designed

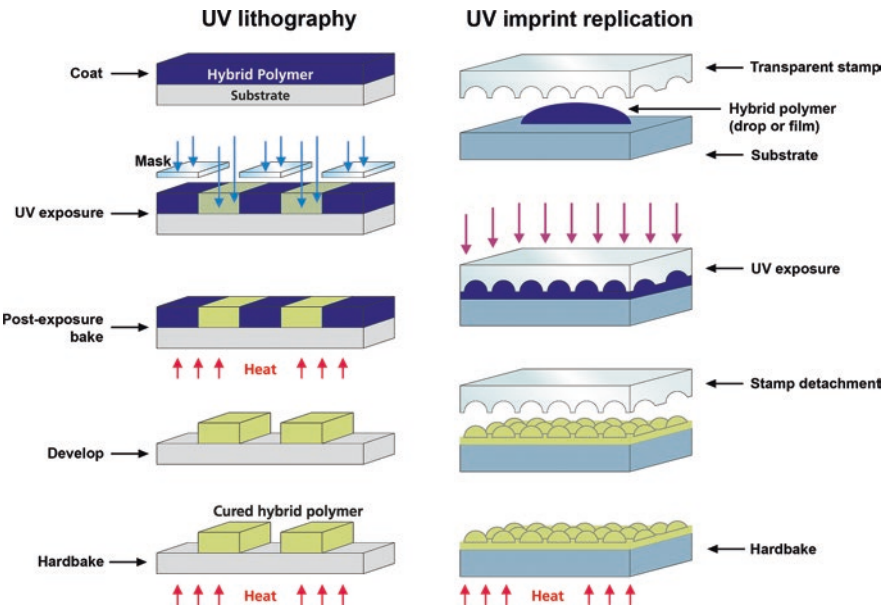


**Fig. 7.3** Process schemes for the wafer-scale direct structuring of hybrid polymers using UV lithography or pattern replication using UV imprinting

to have a broad processing window in terms of wavelengths and intensity used, e.g., broadband UV, i-line (365 nm), or h-line (405 nm) irradiation. However, specific UV curing conditions prevailing, for example, during 3D printing, may require an adaptation of the photoinitiator content or type (*vide infra*). Notably, UV curing of commercial hybrid polymers [25] is based on free radical polymerization of acrylate and methacrylate groups, thus showing very fast curing speeds in the range of seconds to few minutes with low-intensity UV light. This is in contrast to epoxy-based optical polymers, which need significantly longer processing times including thermal steps. Efficient bleaching of the photoinitiator and high conversion of the polymerizable groups leads to absence of yellowing and increased long-term stability of the optical properties.

Inhibition effects by the presence of oxygen during UV curing are typical for free radical polymerizations [40] and strongly depend on the chemistry of the base resin and additives. Notably, formulations such as OrmoComp and OrmoClearFX readily cure under ambient atmosphere and oxygen permeable stamps (e.g., PDMS stamps).

Volume shrinkage of the polymer during curing is of particular importance for the creation of structures with high fidelity and resolution. In general, compared to conventional acrylate polymers, often showing more than 20% volume shrinkage, it is drastically reduced in hybrid polymers due to the preformed inorganic network [29]. Commercial hybrid polymers exhibit shrinkage from 2% up to 7% [25], while in academic work, it has been further reduced to practically zero by incorporation of $ZrO_2$ into the inorganic domain [41].

## *7.2.4 Properties of Hybrid Polymers*

### 7.2.4.1 Optical Transparency

Hybrid polymers for optical applications show full transparency (>99%) for visible wavelengths >400 nm up to the NIR range. Additionally, in the NUV range (350–400 nm), only very little absorption is observed in transmission spectra (Fig. 7.4). Importantly, the outstanding transparency is hardly affected in long-term applications. Post-curing yellowing due to degradation of the polymer backbone by thermal and climate stress, as observed in most purely organic polymers, is minimized by the hybrid structure (*vide infra*). Prerequisites for optimal transparency and low yellowing are the selection of an efficiently bleaching photoinitiator, optimized curing conditions, and careful quality control during synthesis and formulation of the resins concerning selection of raw materials and monitoring of impurities.

With their high optical transparency, low haze and tunable refractive index hybrid polymers are also suited for the application as waveguide materials. Therefore, specifically designed hybrid polymers can be operated with typical datacom wavelengths in the NIR range. Low optical loss at these wavelengths is achieved by two factors:

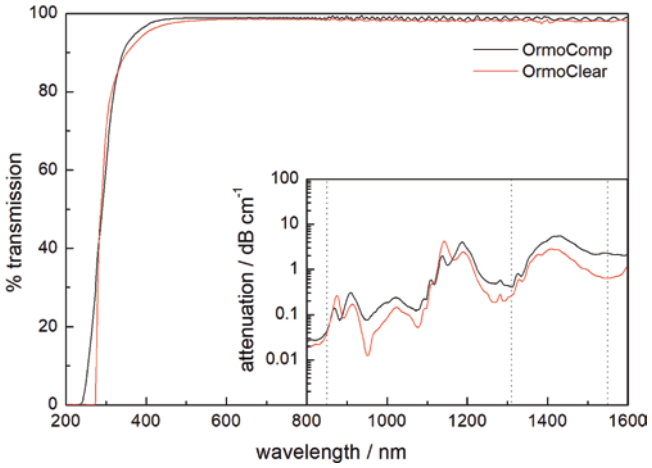


**Fig. 7.4** Optical transmission of cured thin films ($d$ = 20 µm) of hybrid polymers on quartz substrates. Inset: optical attenuation of uncured hybrid polymers in the visible and NIR range

1. Reduction of the CH content in the organic domain by the choice of suited monomers [35]
2. Reduction of the Si–OH content in the inorganic domain by specific, nonaqueous sol-gel conditions [31]

The effect is shown in the inset of Fig. 7.4: the attenuation of uncured OrmoClear, with its low Si–OH-containing base resin, is significantly lower compared to OrmoComp, with its base resin obtained from aqueous sol-gel chemistry. After curing of OrmoClear, its optical attenuation is further reduced to values of 0.2–0.3 dB $cm^{-1}$ at 1310 nm and 0.5–0.6 dB $cm^{-1}$ at 1550 nm [33].

#### 7.2.4.2 Autofluorescence

Autofluorescence of polymers is either intrinsic due to the backbone structure of the polymer or is induced by impurities and degradation phenomena evolving during curing or long-term operation [42]. Notably, the hybrid structure and corresponding stability impose very low levels of autofluorescence to hybrid polymers, in particular OrmoComp and OrmoClearFX [43–46]. With the background signal being comparable to that of Borofloat glass and with its transparency in the NUV and Vis range, these materials are therefore highly suited for the fabrication of cell substrates, optofluidic chips, and imaging probes based on fluorescence detection.

#### 7.2.4.3 Refractive Index and Dispersion

The refractive index of hybrid polymers can be tuned by:

1. Alternation of precursors and conditions of the sol-gel process
2. Chemistry of the organic domain
3. Utilization of other metal alkoxides

In particular the variation of the sol-gel-derived base resin by co-reacting alkoxysilane precursors with $Zr(OR)_4$ or $Ti(OR)_4$ is broadly applied to increase the RI of the resulting hybrid polymers. For commercially available materials and prototypes, currently a range of refractive indices between 1.45 and 1.65 at 589 nm can be realized [25, 30].

For the fabrication of microoptical components, the combination of high refractive index and low dispersion, i.e., high Abbe number, often is desired in order to make structures as compact as possible while keeping acceptable levels of chromatic aberration [14]. However, there is a strict trade-off between the two parameters for organic polymers [15]. As inorganic glass covers significantly wider regions in the Abbe diagram, the combination of inorganic and organic domains [23] in hybrid polymers broadens the achievable refractive index/Abbe number combinations to some extent. Standard hybrid polymers possess Abbe numbers from 30 to 51, depending on the type of material [25].

Compared to conventional organic polymers, hybrid polymers show pronounced negative thermooptical behavior with $dn/dT \sim -2 \cdot 10^{-4}$ $K^{-1}$ and an outstandingly low birefringence in the range of $n_{TE} - n_{TM} < 1$ to $7 \cdot 10^{-4}$. Together with low optical loss (*vide supra*), this makes them good candidates for photonic applications such as thermooptical waveguides or sensors based on microring resonators and Bragg gratings [47–49].

#### 7.2.4.4 Mechanical Properties

By varying the network densities of both the inorganic and organic domains, the mechanical properties such as Young's modulus and coefficient of thermal expansion (CTE) can be tailored over a wide range [29]. Variation of network density is achieved by changing relative amounts of mono-, di-, and trialkoxy silane precursors, the amount of organic polymerizable groups, and the linker length in functionalized organosilanes. With increasing inorganic content and network density, the CTE of hybrid polymers decreases, with typical values being in the range 100–150 ppm $K^{-1}$ for commercial materials [25]. Hybrid polymers possessing Young's modulus from around 100 MPa up to several GPa can be synthesized [29, 32]. Typical values for commercial hybrid polymers for optical applications range between 0.6 and 1.2 GPa [25]. The increased mechanical strength of hybrid polymers in comparison to conventional organic polymers is also manifested in significantly improved scratch and abrasion resistance [30, 50].

#### 7.2.4.5 Thermal and Climate Stability

Hybrid polymers show remarkable stability against physical stress, such as temperature, humidity, and light. Thus, thermogravimetric analysis of hybrid polymers OrmoComp and OrmoClear (Fig. 7.5a) shows beginning decomposition only at temperatures above 360 °C and 300 °C, respectively, which is higher than conventional cross-linkable acrylates. Consequently, these hybrid polymers tolerate long-term heating to 270 °C and short-term heating to 300 °C [25]. Thus, soldering and dicing during subsequent processing of the device can be performed without deterioration of optical properties. Notably, during standardized climate stability tests, in particular temperature cycling and aging under elevated temperature and humidity, hybrid polymers do not show any significant change of their optical characteristics (Fig. 7.5b). Furthermore, under high-intensity irradiation with visible light, hybrid polymers show significantly longer lifetimes than conventional organic UV-curable polymers [33].

#### 7.2.4.6 Biocompatibility

Remarkably high biocompatibility of OrmoComp directly after fabrication of test structures and without any additional surface treatment has been proven in several studies using a number of different cell lines [51–54]. Cell viability on the hybrid polymer is as good as on control substrates. Importantly, UV curing of the substrate should be sufficiently long to reduce the presence of unreacted cytotoxic photoinitiator and acrylates [55]. Furthermore, performing a hardbake after UV curing increases cell viability. In some cases a protein coating [56, 57] or specific functionalization [45] of the OrmoComp surface may be applied to increase cell adherence

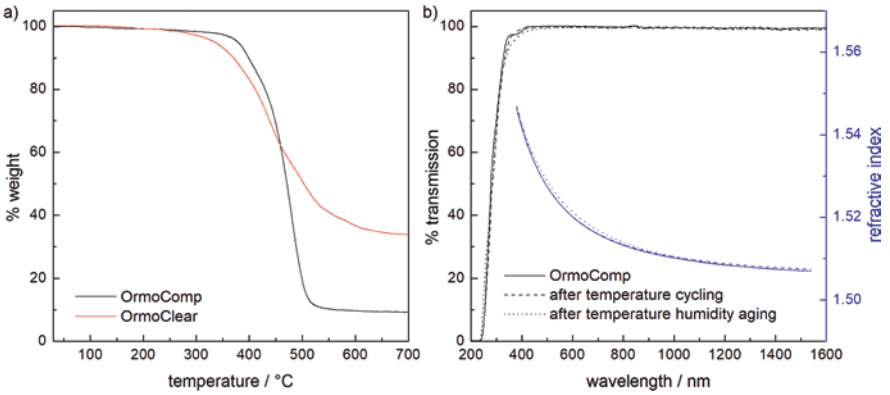


**Fig. 7.5** (**a**) Thermogravimetry of hybrid polymers OrmoComp and OrmoClear. (**b**) Transmission and refractive index dispersion of thin films of OrmoComp ($d$ = 20 µm) before and after temperature cycling (100 cycles between 45 and 85 °C) and temperature humidity aging (85% RH, 85 °C, 1000 h) tests

and viability. Consequently, in addition to their applications as optical materials, hybrid polymers are advantageously used for the fabrication of micro- and optofluidic devices [43, 58–67], medical diagnostics [44, 66], as well as scaffolds for tissue engineering (*vide infra*).

## 7.3 Fabrication of Microoptical Elements by UV Lithography and Replication Using Hybrid Polymers

High-precision and large-scale production of microoptical and photonic components in 2D using wafer-based processing highly profits from the past technological developments in the semiconductor industries. Thus, optical components are manufactured with micro- and nanometer resolution using classic UV lithography and subsequent etching of the structure into silicon or glass [6]. When using UV-curable polymers as optical materials, most microoptical components are fabricated by cost-effective UV imprinting and replication techniques, besides direct structuring via UV lithography or direct laser writing. These standard techniques are advantageously applied to structure hybrid polymers for the fabrication of microoptical components [11, 12]. Notably, due to the wafer-based processing and restrictions during replication steps, fabrication is limited to 2D and 2.5D structures.

### *7.3.1 UV Lithography and Direct Laser Writing*

Employing hybrid polymers as negative-tone resists and their direct patterning using UV lithography and direct laser writing in principle yields binary structures, i.e., a film of the hybrid polymer is fully cured at certain positions and washed away at others during the development step. Consequently, these techniques are mainly utilized for binary photonic structures such as waveguides using OrmoCore and OrmoClad—hybrid polymers specifically designed for waveguide applications [31, 67–70]. Stacks of waveguides were realized by layer-wise repetition of the coating and structuring process [71, 72].

Also nonbinary structures can be realized using combined nanoimprint and UV lithography: by applying a mask pre-structured with an aperture lens on a thick layer of hybrid polymer, an array of high-aspect-ratio conic microlenses was fabricated [34, 73]. By profiting from diffraction effects during proximity exposure, concave microchannels acting as mirror elements were fabricated into OrmoComp, enhancing fluorescent single-cell imaging [62].

Besides these optical and photonic applications, direct structuring of hybrid polymers by UV lithography and direct laser writing is used for fabrication of microfluidic chips [43, 58, 61, 74]. Hybrid polymers may also be used as sacrificial

photoresist in UV lithography for pattern transfer in etching processes with high etch selectivity [75].

### *7.3.2 UV Imprint and Replication*

More complex 2.5D microoptical structures can be fabricated with hybrid polymers using replication from a master stamp by NIL. In particular, structures with high resolution down to few nanometers, combining elements on completely different length scales from nano to micro, or designed as freeform optical elements can be realized, given a properly structured master original is available. The latter may be fabricated by conventional UV lithography, direct laser writing, electron-beam lithography, or focused ion beam milling with high resolution and large freedom in design. However, as master fabrication is very laborious and cost-intensive, it is advantageous to replicate it into a working stamp, which in turn is used to perform multiple imprints into the optical polymer.

In this respect, hybrid polymers offer superior properties not only for the fabrication of microoptical components itself but also for the fabrication of working stamps for their replication. A dedicated commercial material—OrmoStamp—is widely used as hard stamp material suited for thermal and UV-NIL with low oxygen permeability, superior resolution and structure fidelity, as well as high durability during repetitive imprinting processes [76–80].

Microlens arrays constitute one of the most important microoptical elements and are indispensable for imaging and illumination applications in today's scientific and medical instruments and most importantly consumer products [81]. The masters for microlens arrays can be obtained by photolithographic structuring of a photoresist and subsequent thermal reflow to obtain spherical or cylindrical lenses [82, 83]. These structures can be etched into the substrate or transferred by molding into a working stamp. By imprinting into the optical polymer such as OrmoComp, microlens arrays are fabricated directly on CMOS detectors [83] or VCSELs [84] and are implemented into stacks of functional elements within wafer-scale production processes. Low shrinkage and high thermal stability of hybrid polymers (*vide supra*) are advantageous for high structural precision and stability during further handling of functional dies including soldering and dicing at elevated temperatures. Recently microlens arrays were realized by UV imprinting of OrmoComp on flexible fluorinated polymer substrates being suited for roll-to-roll fabrication processes (Fig. 7.6a). Structured foils could be bent to low radii without deterioration of the optical properties of the lenses [85].

NIL fabrication is similarly suited to replicate structures containing features with very different length scales. Thus, macroscopic millimeter-sized lenses containing a nanostructured surface as intrinsic moth-eye antireflective layer could be replicated with excellent structural fidelity into the hybrid polymer OrmoClear (Fig. 7.6b) [11]. The master for the replication process was obtained by combining thermoformed lenses with a nanostructured foil [86]. Similar hierarchically structured

optical elements such as a microlens array with an antireflective layer [87] and a diffusor element with a diffractive nanostructure on top [88] were fabricated by replication into OrmoComp.

Freeform refractive lens arrays utilized as multi-aperture objective for ultra-slim cameras were fabricated using OrmoComp as the optical material (Fig. 7.6c) [89, 90]. As photoresist reflow cannot be applied for master fabrication due to the free-form structure of the lens array, a step-and-repeat process starting from an ultra-precision machined single lens array master was applied to replicate the structure on wafer-scale. For superior quality of the optical surface, the stamp tool was moved in $z$-direction during curing to compensate for shrinkage of the material.

A number of photonic components such as waveguides for datacom applications [91–96] and microring resonators for sensing [47, 97] have been fabricated into low-optical-loss hybrid polymers OrmoClear, OrmoCore, and OrmoClad using UV-NIL. Figure 7.6d shows a microring resonator functioning with high $Q$-factor

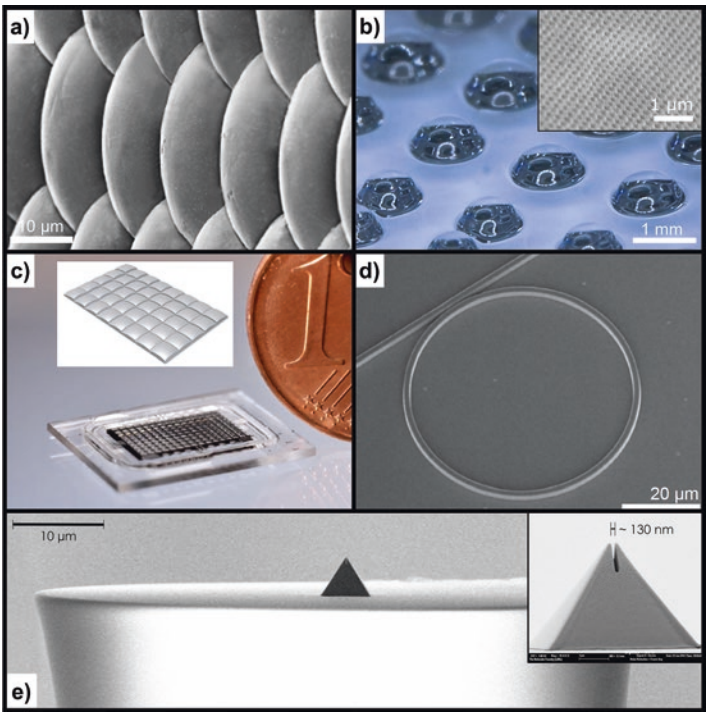


**Fig. 7.6** Examples of replicated microoptical structures by UV imprinting of hybrid polymers: (**a**) SEM micrograph of OrmoComp microlens array on flexible fluorinated ethylene propylene (FEP) substrate [85]. (**b**) OrmoClear macro lenses with nanostructured surface [11]. (**c**) Multi-aperture objective for ultrathin camera modules containing two refractive freeform microlens arrays fabricated using OrmoComp. Inset: 3D model of one quarter of the lens array [90]. (**d**) SEM micrograph of a microring resonator with designed gap width of 250 nm fabricated using OrmoCore [47]. (**e**) SEM micrograph of a campanile probe at the facet of an optical fiber imprinted into OrmoComp [102]

which was fabricated on wafer scale with nanometer resolution. Further examples of NIL replicated photonic structures consist of photonic fences [98], Bragg gratings [48, 49], and metasurfaces [99].

Of particular interest is the generation of photonic nanostructures on the facet of an optical fiber to modify and improve its beam shaping and collecting properties. Thus, a 3D beam splitter, Fresnel lens, and campanile probe were realized by direct nanoimprinting on the facet of a fiber [100–102]. The process includes several molding steps using the hybrid polymer OrmoComp as mold and imprint material. Alignment of the mold and the fiber is guided by red light being coupled into the fiber, while final curing of the structure on the tip is achieved by sending blue light through it. By realizing a nanometer-sized gap on the campanile probe, sub-diffraction imaging was demonstrated (Fig. 7.6e).

## 7.4 Hybrid Polymers in Additive Manufacturing

In contrast to structuring by UV lithography and UV imprinting, which are basically limited to 2.5D structures, additive manufacturing allows for fabrication with full freedom in the three-dimensional space, paving the way for new designs and functions of microoptical components. In addition to wafer-based processing, other substrates, including pre-patterned and 3D-shaped components, can be directly functionalized with microoptical elements. The technological development in fabrication goes hand in hand with development of improved and new materials, which are specifically adapted to the requirements of the numerous 3D printing processes.

Due to the variability of the synthesis of hybrid polymers, they can be easily adapted to multiple 3D printing processes for the fabrication of optics. Thus, extrusion-based methods, such as nozzle extrusion [103] and inkjet printing (see Sect. 7.4.1), as well as vat polymerization methods, such as stereolithography [104–106] and in particular 2PP-DLW (see Sect. 7.4.2), have been employed for the fabrication of microoptical components using hybrid polymers. Notably, the material OrmoComp is very popular in additive manufacturing due to its fast curing kinetics, oxygen insensitivity, acceptable shrinkage, high biocompatibility, as well as excellent optical and mechanical properties.

### *7.4.1 Inkjet Printing and Dispensing*

Inkjet printing and dispensing may be advantageously applied for the fabrication of microlenses and microlens arrays with enhanced performance due to higher structural variability. The processes are easy to implement and can be applied on wafer scale directly on functional dies. Due to the additive nature of the processes, the printing material can be deposited in a highly controlled manner, thus giving precise control over the position, size, and shape of microlenses. Thus, in particular for the

fabrication of individualized lenses, they are cost-effective and fast alternatives to laborious master fabrication using, e.g., diamond machining or UV lithography and thermal reflow.

Inkjet printing of arrays of microlenses using hybrid polymers was demonstrated on glass substrates [107–110]. An inkjet printing compatible formulation of OrmoComp (InkOrmo) was developed by dilution with suited solvents. This ink was deposited in form of individual droplets onto the surface, prebaked to remove the solvent, and finally UV-cured to give spherical microlenses. It was shown that their size and shape, depending on the free energy balance between the droplet formulation, substrate, and surrounding atmosphere, could be tuned by adjusting the surface's hydrophobicity and the number of droplets per microlens.

To widen the structural variety of inkjet-printed microlenses, a process was developed using a surface pre-patterned with pedestals [111, 112]. The size of the pedestal as well as the amount of ink deposited on top defines the shape of the microlens, allowing for precise control over its focal length and numerical aperture.

An improved optical performance was obtained using hybrid polymer materials for both the patterned surface and the microlenses [113]. For this purpose, nanoimprint lithography for the generation of pedestals was combined with inkjet printing of the microlenses (Fig. 7.7a). With three different pedestal sizes, precise and predictable numerical apertures from 0.45 to 0.9 as well as focal lengths between 10 and 100 µm were obtained by simply adjusting the number of droplets on individual pedestals (Fig. 7.7b). Notably, microlenses with varying focal lengths can easily be combined into multifocal microlens arrays (Fig. 7.7c). Single arrays with up to nine different microlenses were demonstrated.

Recently, sophisticated hybrid microoptical components were fabricated on a wafer scale using a combination of UV-NIL, UV lithography, and inkjet printing [114, 115]. By dispensing a hybrid polymer ink on a micro- and nanostructured template, a combination of refractive and diffractive elements in a single microlens was achieved (Fig. 7.8a). First, a nanostructure consisting of a laminar grating with lines and spaces of 500 nm width and 500 nm depth was replicated using an organic NIL resist. Then, a layer of SU-8 with a thickness of 150 µm was deposited on top of the nanoimprinted grating and photolithographically structured. This gave circular confining structures with a diameter of 1000 µm. The resulting resist master was replicated twice to obtain an exact copy using different soft and hard material combinations as mold and substrate (materials A and B; for details see [115]). Thus, replicas, e.g., in hard OrmoComp on silicon wafer or more flexible OrmoClearFX on PC foil, were generated. The hybrid polymer ink was dispensed into the cavities of the replica and soft-baked to release the solvent. Several repetitions of the dispensing and soft-baking steps might be necessary to achieve the final lens shape. The total amount of dispensed hybrid polymer defines the focal length of the refractive part of the microlens. Finally, UV curing, hard-baking, and demolding yield the hybrid refractive-diffractive microlens (Fig. 7.8b). The structural fidelity during the replication processes is very high with shrinkage of the step height below 5% over the whole process chain. Optical testing using a collimated expanded laser beam gave the expected image of three partial beams due to diffraction of the laminar

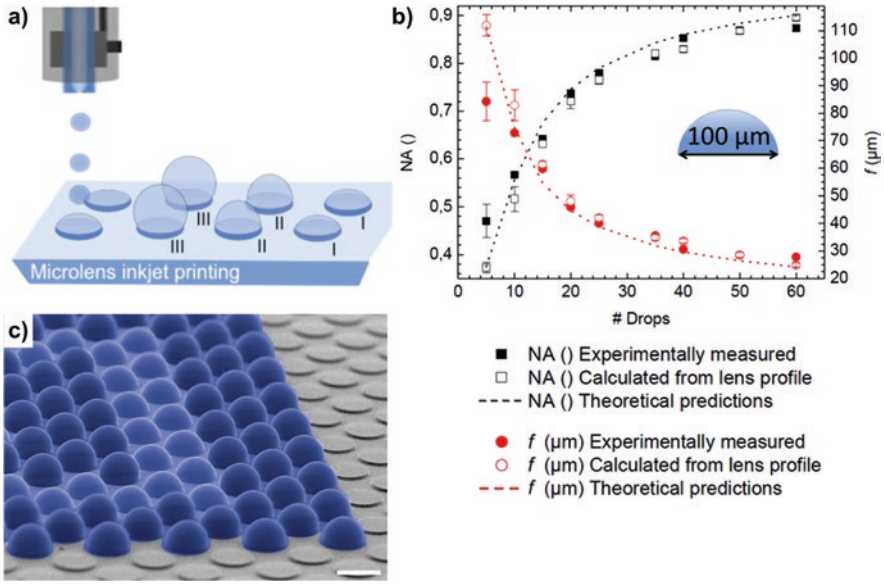


**Fig. 7.7** Inkjet printing of microlenses on preformed pedestals: (**a**) Illustration of the printing process. (**b**) Dependence of numerical aperture and focal length of the lens on amount of dispensed ink in case of 100 µm diameter pedestals. (**c**) Artificially colored SEM micrograph of an array of microlenses with two different focal lengths (scale bar = 100 µm) [113]

grating well-focused by the refractive part of the microlens (Fig. 7.8c). This work demonstrates the power of combining conventional UV lithography and replication techniques for the generation of functional elements, i.e., a diffractive pattern, with inkjet printing as an additive manufacturing process defining the size and shape of the entire microoptical component.

While the abovementioned inkjet printing processes rely on solvent-based hybrid polymer formulations with low viscosities (<25 mPa s), it would be desirable to utilize solvent-free inks, thereby avoiding time-consuming heating and solvent evaporation steps. In one approach [116] the low-viscosity requirement was met by dilution of OrmoComp resin with an acrylate-based reactive diluent at volume contents up to 70%. Thus, large-area microlens arrays could be inkjet printed with minimum deviations of the individual lens geometries and a largely reduced overall processing time compared to solvent-based inks.

By developing a new picoliter dispensing technique, which is capable of dispensing liquids with a wide range of viscosities (200–10,000 mPa s), the fabrication of microlens arrays and single individualized microlenses was demonstrated using undiluted OrmoComp and OrmoClearFX [117]. A small stamp is used to transfer single polymer droplets in picoliter volumes from a reservoir onto a surface or into a preformed cavity. The shape of the resulting microlens is defined by the amount of transferred material, the diameter of the stamp, viscosity of the polymer resin, and hydrophobicity of the substrate. Being able to dispense viscous, undiluted hybrid

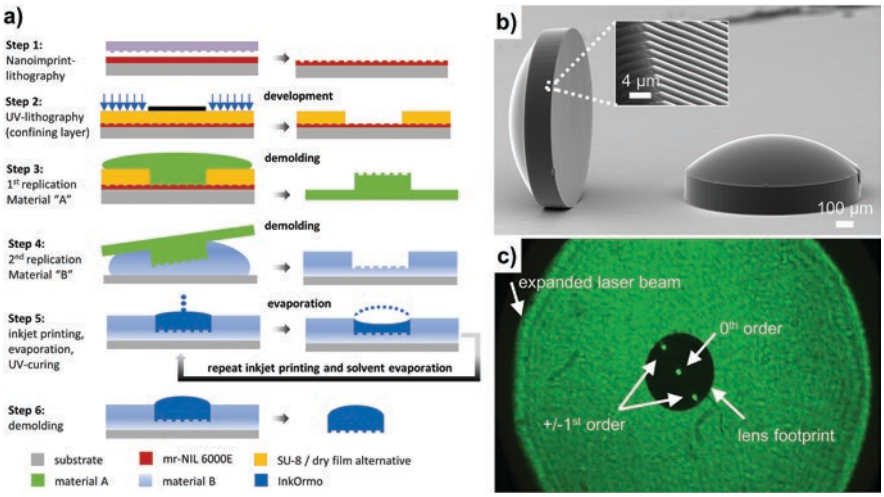


**Fig. 7.8** Refractive-diffractive microlens by combined UV-NIL replication and inkjet printing of hybrid polymers [114, 115]. (**a**) Process chain. (**b**) SEM micrograph of two InkOrmo refractive-diffractive microlenses with a laminar grating as diffractive pattern. (**c**) Screen photograph of the 0th and +/− 1st diffraction orders generated by the diffraction grating and focused by the refractive part of the microlens

polymer resins allows for fast process times and unaltered material properties and thus performance of the fabricated microoptical component.

### *7.4.2 Two-Photon Polymerization Direct Laser Writing (2PP-DLW)*

In recent years 2PP-DLW-based 3D printing developed into an exciting technology for the fabrication of optical components with micro- and nanometer resolution way beyond the diffraction limit of light [118]. 2PP-DLW allows for highest resolutions among today's 3D printing methods, complete architectural freedom in the design of components, fabrication of monolithic materials with smooth surfaces, and the direct printing onto various (functionalized) substrates. A large variety of UV-curable optical materials is utilized for 2PP-DLW [119], among them epoxy-based organic polymers such as SU-8, or more recently mr-DWL, as well as acrylate-based materials such as IP resins (resin formulations optimized to 2PP-DLW proprietary to Nanoscribe GmbH). While these all-organic polymers are optimized for distinct 2PP-DLW processes, their applicability for the fabrication of optical components is limited due to their optical and mechanical properties or stability. Thus, for the fabrication of optical components, using 2PP-DLW direct structuring of hybrid polymers enjoys a tremendous popularity. In particular, the commercially available

OrmoComp and the academia-originated zirconia containing material SZ2080 are widely used and implemented into various 2PP-DLW platforms [120–123].

#### 7.4.2.1 Material Adaptation

Though standard hybrid polymers such as OrmoComp are well suited for 2PP-DLW, specific adaptation of the material to the distinct irradiation conditions can significantly improve the performance [13, 124]. Particularly, the shape accuracy and surface roughness of the printed structures, shrinkage during polymerization, and the usable dynamic range of laser power and scanning speed are important parameters.

It was reported that in a slight modification of the organic curing chemistry, i.e., introducing styrene moieties by the sol-gel process, the resolution of a hybrid polymer resin was significantly improved to the sub-100 nm range [125]. Furthermore, by co-condensation of an organosilane with 20 mol% of zirconium alkoxides $Zr(OR)_4$, a hybrid polymer labeled as SZ2080 was created enjoying much attention in 2PP-DLW 3D printing [41]. Due to its zirconia content, SZ2080 shows negligible shrinkage during polymerization allowing for the fabrication of structures with highest fidelity [126]. Furthermore, damage of the material by high-intensity laser light is significantly reduced broadening the processing window [127, 128]. However, compared to conventional solvent-free hybrid polymers, SZ2080 is a solvent-based formulation; thus spin coating and pre-baking steps to evaporate the solvent are mandatory.

The performance of standard OrmoComp in 2PP-DLW could be further improved by variations in type and content of the photoinitiator as well as content of the stabilizer, generally utilized to prevent premature polymerization in the dark [124]. For nine different formulations, the dynamic range, i.e., the range between the threshold laser power under which no polymerization occurs and overexposure leading to deteriorated shapes and laser damage, was compared (Fig. 7.9a). It turned out that using a photoinitiator with higher two-photon absorption (TPA) cross-section (formulations 1–3) led to lowering of the polymerization threshold but also to reduced resolution and structure fidelity due to the high amount of initiator radicals produced. Increasing the concentration of the standard phosphine oxide photoinitiator (examples 4–6) led to lower threshold values, higher dynamic range, and better structure fidelity (Fig. 7.9b, c). Finally, increasing the concentration of the stabilizer (examples 7–9) led to further improvement of structure fidelity though an increased polymerization threshold was observed. With optimized formulation 9, a complex prism array was realized by 2PP-DLW (Fig. 7.9d), which served as template for the fabrication of a mold and multiple replicas thereof using injection molding [129].

This and other examples [13, 125, 130, 131] show that the performance of a resin in 2PP-DLW is a complex interplay between exposure dose, TPA cross-section of the initiator, radical initiation, and inhibition efficiency as well as polymerization chemistry. Recently it was found that 2PP-DLW with SZ2080 without any added photoinitiator gives structures with improved resolution, surface quality, and stability against laser damage [128]. On the other side, current developments into sophisticated photoinitiators with high TPA cross-section [132] as well as chemical

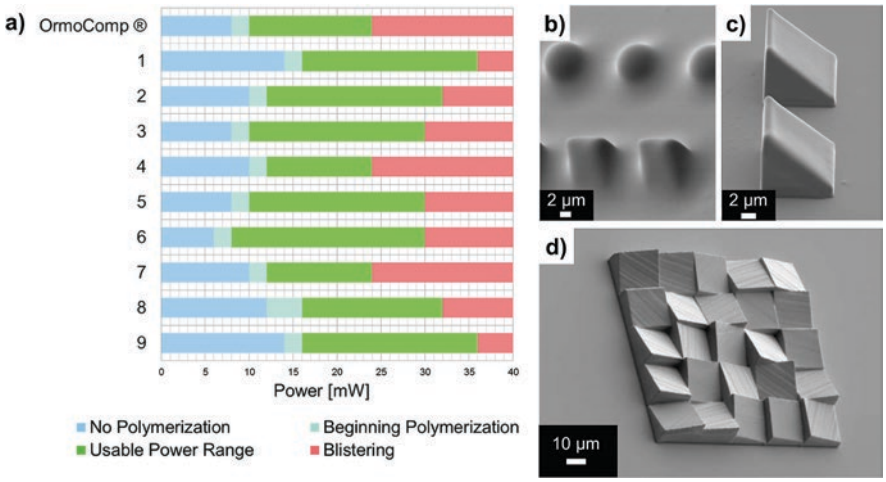


**Fig. 7.9** 3D printing by 2PP-DLW in OrmoComp: (**a**) dynamic range of the usable laser power for standard OrmoComp and nine adapted formulations with tuned photoinitiator and inhibitor content (for details see [124]). (**b**, **c**) SEM micrographs of printed test structures showing the effect of photoinitiator content (0.5% vs. 1.25%) on structure fidelity. (**d**) SEM micrograph of the fabricated prism array with individual inclination and tilt angles of each prism [124]

and instrumental inhibition strategies [133–135] are promising for boosting fabrication speed and attainable resolution of 2PP-DLW.

### 7.4.2.2 Fabrication of Optical Components with 2PP-DLW

Using 2PP-DLW with hybrid polymers, a broad range of optical and photonic components reaching from the nano- to the macroscale have been realized [118, 136]: spherical, axicon, and freeform lenses [66, 137–145], phase plates [146, 147], Fresnel lenses [13, 140], gratings [148], DOEs [140, 149], waveguides [13, 140, 150], photonic fences [98], microcavities [151, 152], photonic crystals [41, 153–155], and metasurfaces [156]. These examples demonstrate that with 2PP-DLW, almost no limitation in shape or size of the architecture exists. An exemplary selection of structures with differing length scales is given in Fig. 7.10.

Particularly remarkable is the fabrication of optics with high resolution and smooth surfaces directly on functional elements: OrmoComp was used to print spherical collimation lenses of different sizes directly onto the facet of an optical fiber (Fig. 7.10a) [141]. Though a layer-wise printing process was utilized, the surface of the lens is smooth, and excellent light output was achieved with the material. The same groups demonstrated printing of a variety of fully freeform structures and compound lenses onto optical fibers and sensor chips using OrmoComp and IP-S resins [141, 157, 158]. Recently, a microlens cascade fabricated from IP-S and OrmoComp using 2PP-DLW was integrated into a functional microendoscopic probe for high-resolution deep tissue imaging [66].

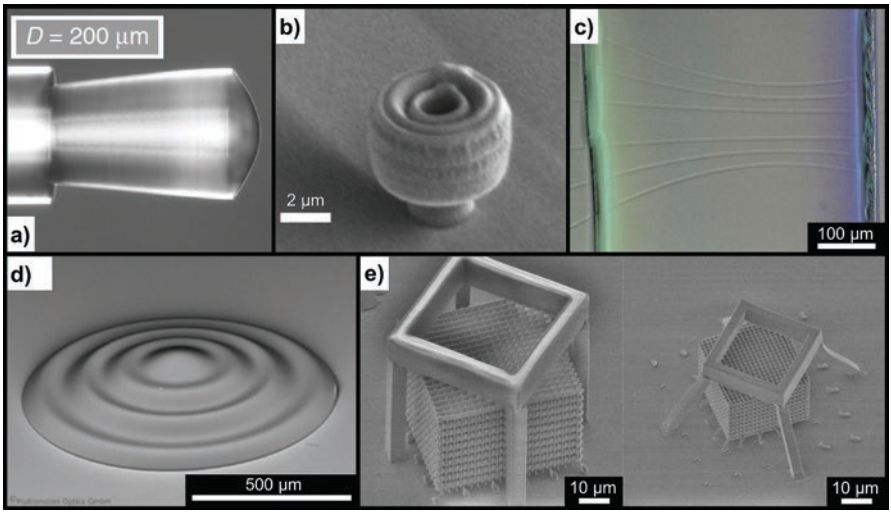


**Fig. 7.10** Microoptical components fabricated by 2PP-DLW using hybrid polymers: (**a**) spherical collimation lens made of OrmoComp on facet of single-mode optical fiber [141]. (**b**) Freeform light-directing nanophotonic lens printed form OrmoComp on top of GaAs nanowire [144]. (**c**) Optical microscope image of six waveguide cores embedded in a cladding matrix of an adapted ORMOCER-based hybrid polymer [13]. (**d**) Millimeter-sized freeform lens fabricated by contour structuring of OrmoComp [145]. (**e**) Photonic crystal structure made of SZ2080 before (left) and after (right) pyrolysis [159]

A remarkable resolution was achieved using standard OrmoComp for fabrication of a nanophotonic lens on emitting GaAs nanowire (Fig. 7.10b) [144]. An evolutionary algorithm was utilized to design the lens structure with nanometer-sized features. By interference effects the isotropic photoluminescence of the GaAs nanowire was turned into highly directional emission over a broad spectral range. The designed structure could be fabricated with high fidelity by 2PP-DLW. The excellent transparency and low autofluorescence of OrmoComp allowed the experimental demonstration of the dramatic angular redistribution of emitted light.

For beam shaping and light distribution applications, instead of sculpturing the surface of a material with a homogeneous refractive index, an alternative approach would be to have a uniform structure and vary the refractive index within. Such a GRIN (gradient refractive index) element was realized using SZ2080 [160]. Within the broad dynamic range of this polymer, the double-bond conversion and similarly the refractive index increases with the laser exposure dose. Thus, by varying scanning speed during 2PP-DLW fabrication, the refractive index was dynamically modulated with a maximum change of $\Delta n = 0.01$ within a single structure.

The dependence of refractive index on exposure dose was further exploited to demonstrate straightforward coupling of optoelectronic components by 2PP-DLW fabrication of waveguides in a cladding matrix. For this purpose, a uniform film of a hybrid polymer resin is coated onto the optoelectronic components, the whole film is cured by UV flash illumination, and finally waveguides are written within the cured material by 2PP-DLW, locally promoting further polymerization and an

increase in refractive index. The principle was demonstrated by fabrication of waveguides between two glass slides in a film of an OrmoComp formulation adapted to 2PP-DLW having a large processing window (Fig. 7.10c) [13]. As the voxel diameter of the writing laser is smaller than the waveguide profile, different sizes (single vs. multimode) and shapes (circular, square, and elliptical) were realized by hatching of the waveguide's cross-section [140]. Importantly, such hybrid polymer waveguides integrated into functional chips are sufficiently stable to survive further lamination, bonding, and dicing steps [161]. Similar to refractive index, the mechanical properties of hybrid polymers change with increasing curing time. Thus, domains with differing elasticity and stiffness may be imparted to a single structure by varying exposure dose [13]. However, close to the polymerization threshold, structures become weak, show much higher shrinkage, and tend to collapse [126, 128, 155].

A common bottleneck in 2PP-DLW fabrication is the limitation in size of the fabricated objects as well as production time. However, recent improvements of instrument manufacturers and the application of sophisticated laser focusing and scanning strategies allowed for significant improvements of both parameters [145]. As an example, the macroscopic ($d$ = 1 mm) freeform lens shown in Fig. 7.10e was rapidly manufactured from OrmoComp using contouring exposure, i.e., the outer shape of the lens was polymerized with the laser, and only after the development step, the inner volume was cured using UV flood illumination. Importantly, for high-throughput 2PP-DLW printing, the materials have to show high reactivity to keep up with the fast laser trajectories. More information on recent developments in 2PP-DLW hardware and processes can be found in Chap. 5 of this book.

The unique combination of inorganic and organic domains in hybrid polymers offers an additional processing step after fabrication of the 3D-printed structure: by pyrolysis and sintering at temperatures above 1000 °C, the organic domain decomposes leaving behind an amorphous inorganic glass or ceramic structure [162, 163]. Therefore, the structure undergoes considerable isotropic shrinkage lowering the minimum structural feature size. Applied to a photonic crystal fabricated with SZ2080, pyrolysis at 1000 °C for 2 h gave shrinkage of ca 40%, while the material stayed amorphous with good structural fidelity (Fig. 7.10d) [128, 159]. Pyrolysis at higher temperatures gave transition into crystalline phases accompanied by deterioration of the structure. Much milder thermal annealing of a hybrid polymer photonic crystal at 300 °C resulted in only partly decomposition of the organic groups further densifying the material. Thus, precise control over shrinkage was achieved resulting in a shift of the photonic band gap from the NIR into the visible range [154].

#### 7.4.2.3 Fabrication of Cell Scaffolds and Microfluidic Devices by 2PP-DLW

Besides optical components, 2PP-DLW of hybrid polymers is widely used for the fabrication of microfluidic structures as well as scaffolds for cell adhesion and tissue engineering. Again OrmoComp plays a remarkable role as a material with

excellent structuring capability being at the same time highly biocompatible, generally without any additional coating step (see Sect. 7.2.4). Additionally, its negligible autofluorescence makes it superior over other 3D printing materials concerning imaging of fluorescently labeled biological structures.

Consequently, 2PP-DLW-derived scaffolds made of OrmoComp are utilized for studying cell adhesion, growth, migration, and differentiation. To this purpose a large variety of patterned surfaces and complex 3D architectures have been realized [54–56, 164–167]. As an example a tubular microtower for the cultivation of neuronal cells is shown in Fig. 7.11a. Precisely controlled surface properties such as wetting behavior, mechanical stiffness of the structure, as well as structural confinements strongly influence cell behavior.

Interestingly, 3D scaffolds made of two or three different materials with distinct binding properties were realized using consecutive printing steps [57, 168, 169]. OrmoComp, showing high tendency to bind proteins, was combined with a photoactivatable and a protein-repellent acrylate resist. Thus, the spatial functionalization of the scaffold with different proteins and subsequent controlled and type-specific adhesion of cells was realized (Fig. 7.11b) [57].

While micrometer-scaled fluidic devices generally are fabricated using molding, imprinting, or one-photon 3D printing, specific fluidic elements requiring nanometer resolution can be created using 2PP-DLW. As such sophisticated elements actively generating microfluidic currents [170–172] as well as arrays of microneedles with different shapes and high aspect ratios used for drug delivery (Fig. 7.11c) [51, 52, 63, 173] were realized using OrmoComp. These applications profit from exceptionally high inertness, biocompatibility, and mechanical strength of the material.

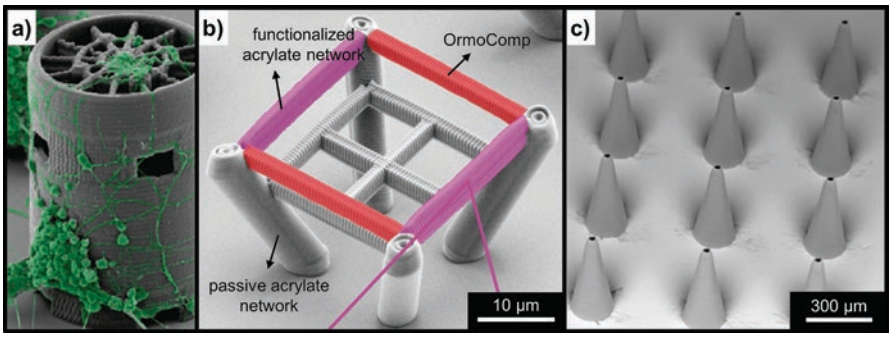


**Fig. 7.11** SEM micrographs of 2PP-DL-printed structures for tissue engineering and medical applications. (**a**) Tubular microtower ($h$ = 150 µm) fabricated form OrmoComp as 3D platform for the cultivation of neuronal cells [166]. (**b**) Multimaterial 3D cell scaffold selectively functionalized with two distinct adhesive proteins (highlighted in red and pink color) for the guidance of cell attachment [57]. (**c**) Array of microneedles fabricated with OrmoComp. Printing of microneedles directly on top of microfluidic channels fabricated in PMMA was demonstrated for the realization of point-of-care systems [63]

## 7.5 Conclusions

Hybrid polymers were demonstrated to be a superior material platform for the manufacturing of reliable and high-performance microoptical components. With their unique structure, derived from the combination of inorganic glass-like with organic polymeric domains in one material, hybrid polymers unify excellent optical properties, environmental stability, and versatility in processing. Importantly, by adaptation of chemical synthesis, formulation, and processing conditions, the properties of hybrid polymers can be tuned over a broad range and tailored to specific applications.

By wafer-scale processing of hybrid polymers using UV lithography and nanoimprint lithography, sophisticated microoptical components are routinely manufactured with high precision, high throughput, and low costs. Synthesis of hybrid polymers and their processing employing these technologies are established in industrial environments serving markets, for example, in consumer electronics, telecommunication, and lighting and sensing applications.

Additive manufacturing and 3D printing of microoptics brings new perspectives for the design of optical elements as well as their fabrication, such as exploitation of all three dimensions and rapid prototyping. The ever-increasing number of additive manufacturing processes and their technological advance require specific adaptations of materials to be printed in order to gain best performance in terms of quality and throughput. Besides their commercial applications in wafer-level optics, hybrid polymers are perfectly suited for additive manufacturing of optical and other components, in particular using inkjet printing and 2PP-DLW. Therefore, we foresee the utility of hybrid polymers in the direct fabrication of individualized microoptical components with high demands on optical and mechanical properties as well as environmental and long-term stability.

A current challenge in the development of hybrid polymers as optical materials consists of extending the range of achievable refractive indices and dispersion without deteriorating the optical performance and reliability. Specific challenges related to additive manufacturing are the adaptation of hybrid polymer resins to low-viscosity requirements, as set by, e.g., inkjet printing, as well as the precise tailoring of optical density, curing speed, shrinkage, and oxygen sensitivity, as required by laser-assisted 3D printing methods. Fine-tuning of these parameters by resin synthesis and formulation utilizing sophisticated chemical concepts enables large improvements in writing speed and resolution [174–176]. In addition, the simultaneous additive processing of multiple materials with different mechanical and optical properties [177] and implementation of special material functions becoming active after fabrication [178–180] hold great promise for future developments.

We actively pursue the development of hybrid polymers towards these directions in order to improve established applications and help to create exciting innovations in microoptics and related fields.

## References


1. Salt, M., & Rossi, M. (2006). Replicated micro-optics for multimedia products. *Proceedings of SPIE, 6196*, 61960F.
2. Duparré, J., & Völkel, R. (2006). Novel optics/micro-optics for miniature imaging systems. *Proceedings of SPIE, 6196*, 619607a.
3. Zappe, H. (2012). Micro-optics: A micro-tutorial. *Advanced Optical Technologies, 1*, 117–126.
4. Mönch, W. (2015). Micro-optics in lighting applications. *Advanced Optical Technologies, 4*, 79–85.
5. Kress, B. C. (2019). Digital optical elements and technologies (EDO19): Applications to AR/VR/MR. *Proceedings of SPIE, 11062*, 1106222.
6. Völkel, R. (2012). Wafer-scale micro-optics fabrication. *Advanced Optical Technologies, 1*, 135–150.
7. Camposeo, A., Persano, L., Farsari, M., & Pisignano, D. (2019). Additive manufacturing: Applications and directions in photonics and optoelectronics. *Advanced Optical Materials, 7*, 1800419.
8. Kotz, F., Arnold, K., Bauer, W., Schild, D., Keller, N., Sachsenheimer, K., Nargang, T. M., Richter, C., Helmer, D., & Rapp, B. E. (2017). Three-dimensional printing of transparent fused silica glass. *Nature, 544*, 337–339.
9. Nguyen, D. T., Meyers, C., Yee, T. D., Dudukovic, N. A., Destino, J. F., Zhu, C., Duoss, E. B., Baumann, T. F., Suratwala, T., Smay, J. E., & Dylla-Spears, R. (2017). 3D-printed transparent glass. *Advanced Materials, 29*, 1701181.
10. Gal-Or, E., Gershoni, Y., Scotti, G., Nilsson, S. M. E., Saarinen, J., Jokinen, V., Strachan, C. J., af Gennäs, G. B., Yli-Kauhaluoma, J., & Kotiaho, T. (2019). Chemical analysis using 3D printed glass microfluidics. *Analytical Methods, 11*, 1802–1810.
11. Grützner, G., Klein, J., Vogler, M., & Schleunitz, A. (2014). UV-curable hybrid polymers for optical applications: Technical challenges, industrial solutions, and future developments. *Proceedings of SPIE, 8974*, 897406.
12. Schleunitz, A., Klein, J. J., Houbertz, R., Vogler, M., & Grützner, G. (2015). Towards high precision manufacturing of 3D optical components using UV-curable hybrid polymers. *Proceedings of SPIE, 9368*, 93680E.
13. Schleunitz, A., Klein, J. J., Krupp, A., Stender, B., Houbertz, R., & Grützner, G. (2017). Evaluation of hybrid polymers for high-precision manufacturing of 3D optical interconnects by two-photon absorption lithography. *Proceedings of SPIE, 10109*, 1010905.
14. Hartmann, P., Jedamzik, R., Reichel, S., & Schreder, B. (2010). Optical glass and glass ceramic historical aspects and recent developments: A Schott view. *Applied Optics, 49*, D157–D176.
15. Brinkmann, M., Hayden, J., Letz, M., Reichel, S., Click, C., Mannstadt, W., Schreder, B., Wolff, S., Ritter, S., Davis, M., Bauer, T., Ren, H., Fan, Y.-H., Wu, S.-T., Bonrad, K., Krätzig, E., Buse, K., & Paquin, R. (2007). Optical materials and their properties. In F. Träger (Ed.), *Springer hand-book of lasers and optics* (pp. 249–372). New York, NY: Springer.
16. Tagaya, A., & Koike, Y. (2012). Compensation and control of the birefringence of polymers for photonics. *Polymer Journal, 44*, 306–314.
17. Schaub, M. P. (2012). A tutorial on plastic consumer optics. *Advanced Optical Technologies, 1*, 21–29.
18. Schift, H. (2008). Nanoimprint lithography: An old story in modern times? A review. *Journal of Vacuum Science and Technology B, 26*, 458–480.
19. Schift, H. (2014) *NaPANIL library of processes* (3rd ed.), published by the NaPANIL-consortium represented by J. Ahopelto, ISBN: 978-3-00-038372-4. Retrieved from http://www.psi.ch/lmn/helmut-schift
20. Ligon, S. C., Liska, R., Stampfl, J., Gurr, M., & Mülhaupt, R. (2017). Polymers for 3D printing and customized additive manufacturing. *Chemical Reviews, 117*, 10212–10290.

21. Sanchez, C., Julián, B., Belleville, P., & Popall, M. (2005). Applications of hybrid organic–inorganic nanocomposites. *Journal of Materials Chemistry, 15*, 3559–3592.
22. Lebeau, B., & Innocenzi, P. (2011). Hybrid materials for optics and photonics. *Chemical Society Reviews, 40*, 886–906.
23. Werdehausen, D., Burger, S., Staude, I., Pertsch, T., & Decker, M. (2019). Nanocomposites—A Route to better and smaller optical Elements? In *Proceedings of OSA Optical Design and Fabrication* (p. OT2A.2). Washington, DC: Optical Society of America.
24. Trademark of the Fraunhofer-Gesellschaft zur Förderung der angewandten Forschung e.V. München.
25. Hybrid polymers manufactured by micro resist technology GmbH. Retrieved from https://www.microresist.com
26. Schmidt, H., Scholze, H., & Kaiser, A. (1984). Principles of hydrolysis and condensation reaction of alkoxysilanes. *Journal of Non-Crystalline Solids, 63*, 1–11.
27. Schmidt, H., & Seiferling, B. (1986). Chemistry and applications of inorganic-organic polymers (organically modified silicates). *MRS Proceedings, 73*, 739.
28. Schmidt, H., & Wolter, H. (1990). Organically modified ceramics and their applications. *Journal of Non-Crystalline Solids, 121*, 428–435.
29. Haas, K.-H., & Wolter, H. (1999). Synthesis, properties and applications of inorganic–organic copolymers (ORMOCER®s). *Current Opinion in Solid State & Materials Science, 4*, 571–580.
30. Haas, K.-H. (2000). Hybrid inorganic–organic polymers based on organically modified sialkoxides. *Advanced Engineering Materials, 2*, 571–582.
31. Buestrich, R., Kahlenberg, F., Popall, M., Dannberg, P., Müller-Fiedler, R., & Rösch, O. (2001). ORMOCER®s for optical interconnection technology. *Journal of Sol-Gel Science and Technology, 20*, 181–186.
32. Haas, K.-H., & Rose, K. (2003). Hybrid inorganic/organic polymers with nanoscale building blocks: Precursors, processing, properties and applications. *Reviews on Advanced Materials Science, 5*, 47–52.
33. Houbertz, R., Domann, G., Cronauer, C., Schmitt, A., Martin, H., Park, J.-U., Fröhlich, L., Buestrich, R., Popall, M., Streppel, U., Dannberg, P., Wächter, C., & Bräuer, A. (2003). Inorganic–organic hybrid materials for application in optical devices. *Thin Solid Films, 442*, 194–200.
34. Houbertz, R., Fröhlich, L., Popall, M., Streppel, U., Dannberg, P., Bräuer, A., Serbin, J., & Chichkov, B. N. (2003). Inorganic–organic hybrid polymers for information technology: From planar technology to 3D nanostructures. *Advanced Engineering Materials, 5*, 551–555.
35. Kahlenberg, F., & Popall, M. (2004). ORMOCER®s (organic-inorganic hybrid polymers) for telecom applications: Structure/property correlations. *MRS Online Proceeding Library Archive, 847*, EE14.4.
36. Schubert, U. (2015). Chemistry and fundamentals of the sol–gel process. In D. Levy & M. Zayat (Eds.), *The sol-gel handbook* (pp. 1–28). New York: Wiley.
37. Schubert, U. (2018). Sol-Gel-Chemie. *Chemie in unserer Zeit, 52*, 18–25.
38. Fessel, S., Schneider, A. M., Steenhusen, S., Houbertz, R., & Behrens, P. (2012). Towards an atomistic model for ORMOCER®-I: Application of forcefield methods. *Journal of Sol-Gel Science and Technology, 63*, 356–365.
39. Green, W. A. (2010). *Industrial photoinitiators: A technical guide*. Boca Raton: CRC Press.
40. Ligon, S. C., Husár, B., Wutzel, H., Holman, R., & Liska, R. (2014). Strategies to reduce oxygen inhibition in photoinduced polymerization. *Chemical Reviews, 114*, 557–589.
41. Ovsianikov, A., Viertl, J., Chichkov, B., Oubaha, M., MacCraith, B., Sakellari, I., Giakoumaki, A., Gray, D., Vamvakaki, M., Farsari, M., & Fotakis, C. (2008). Ultra-low shrinkage hybrid photosensitive material for two-photon polymerization microfabrication. *ACS Nano, 2*, 2257–2262.
42. Piruska, A., Nikcevic, I., Lee, S. H., Ahn, C., Heineman, W. R., Limbach, P. A., & Seliskar, C. J. (2005). The autofluorescence of plastic materials and chips measured under laser irradiation. *Lab on a Chip, 5*, 1348–1354.

43. Sikanen, T., Aura, S., Heikkilä, L., Kotiaho, T., Franssila, S., & Kostiainen, R. (2010). Hybrid ceramic polymers: New, nonbiofouling, and optically transparent materials for microfluidics. *Analytical Chemistry, 82*, 3874–3882.
44. Tadayon, M. A., Pavlova, I., Martyniuk, K. M., Mohanty, A., Roberts, S. P., Barbosa, F., Denny, C. A., & Lipson, M. (2018). Microphotonic needle for minimally invasive endoscopic imaging with sub-cellular resolution. *Scientific Reports, 8*, 10756.
45. Kidwell, D. A., Lee, W.-K., Perkins, K., Gilpin, K. M., O'Shaughnessy, T. J., Robinson, J. T., Sheehan, P. E., & Mulvaney, S. P. (2019). Chemistries for making additive nanolithography in OrmoComp permissive for cell adhesion and growth. *ACS Applied Materials & Interfaces, 11*, 19793–19798.
46. Schmid, M., Ludescher, D., & Giessen, H. (2019). Optical properties of photoresists for femtosecond 3D printing: Refractive index, extinction, luminescence-dose dependence, aging, heat treatment and comparison between 1-photon and 2-photon exposure. *Optical Materials Express, 9*, 4564–4577.
47. Kirchner, R., Finn, A., Landgraf, R., Nueske, L., Teng, L., Vogler, M., & Fischer, W. (2014). Direct UV-imprinting of hybrid-polymer photonic microring resonators and their characterization. *Journal of Lightwave Technology, 32*, 1674–1681.
48. Foerthner, M., Rumler, M., Stumpf, F., Fader, R., Rommel, M., Frey, L., Girschikofsky, M., Belle, S., Hellmann, R., & Klein, J. J. (2016). Hybrid polymers processed by substrate conformal imprint lithography for the fabrication of planar Bragg gratings. *Applied Physics A: Materials Science & Processing, 122*, 240.
49. Förthner, M., Girschikofsky, M., Rumler, M., Stumpf, F., Rommel, M., Hellmann, R., & Frey, L. (2018). One-step nanoimprinted Bragg grating sensor based on hybrid polymers. *Sensors and Actuators A: Physical, 283*, 298–304.
50. Schottner, G., Rose, K., & Posset, U. (2003). Scratch and abrasion resistant coatings on plastic lenses—State of the art, current developments and perspectives. *Journal of Sol-Gel Science and Technology, 27*, 71–79.
51. Doraiswamy, A., Jin, C., Narayan, R. J., Mageswaran, P., Mente, P., Modi, R., Auyeung, R., Chrisey, D. B., Ovsianikov, A., & Chichkov, B. (2006). Two photon induced polymerization of organic-inorganic hybrid biomaterials for microstructured medical devices. *Acta Biomaterialia, 2*, 267–275.
52. Doraiswamy, A., Ovsianikov, A., Gittard, S. D., Monteiro-Riviere, N. A., Crombez, R., Montalvo, E., Shen, W., Chichkov, B. N., & Narayan, R. J. (2010). Fabrication of microneedles using two photon polymerization for transdermal delivery of nanomaterials. *Journal of Nanoscience and Nanotechnology, 10*, 6305–6312.
53. Yoon, S.-H., Kim, Y. K., Han, E. D., Seo, Y.-H., Kim, B. H., & Mofrad, M. R. K. (2012). Passive control of cell locomotion using micropatterns: The effect of micropattern geometry on the migratory behavior of adherent cells. *Lab on a Chip, 12*, 2391–2402.
54. Ovsianikov, A., Schlie, S., Ngezahayo, A., Haverich, A., & Chichkov, B. N. (2007). Two-photon polymerization technique for microfabrication of CAD-designed 3D scaffolds from commercially available photosensitive materials. *Journal of Tissue Engineering and Regenerative Medicine, 1*, 443–449.
55. Trautmann, A., Rüth, M., Lemke, H.-D., Walther, T., & Hellmann, R. (2018). Two-photon polymerization based large scaffolds for adhesion and proliferation studies of human primary fibroblasts. *Optics and Laser Technology, 106*, 474–480.
56. Turunen, S., Käpylä, E., Lähteenmäki, M., Ylä-Outinen, L., Narkilahti, S., & Kellomäki, M. (2014). Direct laser writing of microstructures for the growth guidance of human pluripotent stem cell derived neuronal cells. *Optics and Lasers in Engineering, 55*, 197–204.
57. Richter, B., Hahn, V., Bertels, S., Claus, T. K., Wegener, M., Delaittre, G., Barner-Kowollik, C., & Bastmeyer, M. (2017). Guiding cell attachment in 3D microscaffolds selectively functionalized with two distinct adhesion proteins. *Advanced Materials, 29*, 1604342.
58. Aura, S., Sikanen, T., Kotiaho, T., & Franssila, S. (2008). Novel hybrid material for microfluidic devices. *Sensors and Actuators B: Chemical, 132*, 397–403.

59. Fernandez-Cuesta, I., Laura Palmarelli, A., Liang, X., Zhang, J., Dhuey, S., Olynick, D., & Cabrini, S. (2011). Fabrication of fluidic devices with 30 nm nanochannels by direct imprinting. *Journal of Vacuum Science and Technology B, 29*, 06F801.
60. Sikanen, T., Aura, S., Franssila, S., Kotiaho, T., & Kostiainen, R. (2012). Microchip capillary electrophoresis-electrospray ionization–mass spectrometry of intact proteins using uncoated Ormocomp microchips. *Analytica Chimica Acta, 711*, 69–76.
61. Singh, A., Scotti, G., Sikanen, T., Jokinen, V., & Franssila, S. (2014). Laser direct writing of thick hybrid polymers for microfluidic chips. *Micromachines, 5*, 472–485.
62. Bonabi, A., Cito, S., Tammela, P., Jokinen, V., & Sikanen, T. (2017). Fabrication of concave micromirrors for single cell imaging via controlled over-exposure of organically modified ceramics in single step lithography. *Biomicrofluidics, 11*, 034118.
63. Trautmann, A., Roth, G.-L., Nujiqi, B., Walther, T., & Hellmann, R. (2019). Towards a versatile point-of-care system combining femtosecond laser generated microfluidic channels and direct laser written microneedle arrays. *Microsystems & Nanoengineering, 5*, 6.
64. Fernandez-Cuesta, I., West, M. M., Montinaro, E., Schwartzberg, A., & Cabrini, S. (2019). A nanochannel through a plasmonic antenna gap: An integrated device for single particle counting. *Lab on a Chip, 19*, 2394–2403.
65. Esmek, F. M., Bayat, P., Pérez-Willard, F., Volkenandt, T., Blick, R. H., & Fernandez-Cuesta, I. (2019). Sculpturing wafer-scale nanofluidic devices for DNA single molecule analysis. *Nanoscale, 11*, 13620–13631.
66. Tadayon, M. A., Chaitanya, S., Martyniuk, K. M., McGowan, J. C., Roberts, S. P., Denny, C. A., & Lipson, M. (2019). 3D microphotonic probe for high resolution deep tissue imaging. *Optics Express, 27*, 22352–22362.
67. Mohamed, R., Razali, N., Ehsan, A. A., & Shaari, S. (2005). Characterisation and process optimisation of photosensitive acrylates for photonics applications. *Science and Technology of Advanced Materials, 6*, 375–382.
68. Rezzonico, D., Guarino, A., Herzog, C., Jazbinsek, M., & Günter, P. (2006). High-finesse laterally coupled organic-inorganic hybrid polymer microring resonators for VLSI photonics. *IEEE Photonics Technology Letters, 18*, 865–867.
69. Wang, S., Borden, B., Li, Y., & Goel, P. (2006). Laser direct writing of inorganic-organic hybrid polymeric channel waveguide for optical integrated circuits. *Proceedings of SPIE, 6389*, 63890B.
70. Madani, A., & Azarinia, H. R. (2017). Design and fabrication of all-polymeric photonic waveguides in optical integrated circuits. *Optik, 138*, 33–39.
71. Streppel, U., Dannberg, P., Wächter, C., Bräuer, A., Nicole, P., Fröhlich, L., Houbertz, R., & Popall, M. (2001). Development of a new fabrication method for stacked optical waveguides using inorganic-organic copolymers. In *Proc. IEEE Conference on Polymers and Adhesives in Microelectronics and Photonics* (pp. 329–335).
72. Streppel, U., Dannberg, P., Wächter, C., Bräuer, A., Fröhlich, L., Houbertz, R., & Popall, M. (2003). New wafer-scale fabrication method for stacked optical waveguide interconnects and 3D micro-optic structures using photoresponsive (inorganic–organic hybrid) polymers. *Optical Materials, 21*, 475–483.
73. Streppel, U., Dannberg, P., Wächter, C., Bräuer, A., & Kowarschik, R. (2003). Formation of micro-optical structures by self-writing processes in photosensitive polymers. *Applied Optics, 42*, 3570–3579.
74. Järvinen, P., Bonabi, A., Jokinen, V., & Sikanen, T. (2020). Simultaneous culturing of cell monolayers and spheroids on a single microfluidic device for bridging the gap between 2D and 3D cell assays in drug research. *Advanced Functional Materials, 30*, 2000479.
75. Tsougeni, K., Bourkoula, A., Petrou, P., Tserepi, A., Kakabakos, S. E., & Gogolides, E. (2014). Photolithography and plasma processing of polymeric lab on chip for wetting and fouling control and cell patterning. *Microelectronic Engineering, 124*, 47–52.
76. Klukowska, A., Vogler, M., Kolander, A., Reuther, F., Grützner, G., Mühlberger, M., Bergmair, I., & Schöftner, R. (2008). Alternative approach to transparent stamps for UV-based nanoimprint lithography—Techniques and materials. *Proceedings of SPIE*, *6792*, 67920J.

77. Schift, H., Spreu, C., Saidani, M., Bednarzik, M., Gobrecht, J., Klukowska, A., Reuther, F., Grützner, G., & Solak, H. (2009). Transparent hybrid polymer stamp copies with sub-50-nm resolution for thermal and UV-nanoimprint lithography. *Journal of Vacuum Science and Technology B, 27*, 2846–2849.
78. Schleunitz, A., Spreu, C., Mäkelä, T., Haatainen, T., Klukowska, A., & Schift, H. (2011). Hybrid working stamps for high speed roll-to-roll nanoreplication with molded sol–gel relief on a metal backbone. *Microelectronic Engineering, 88*, 2113–2116.
79. Schleunitz, A., Vogler, M., Fernandez-Cuesta, I., Schift, H., & Grützner, G. (2013). Innovative and tailor-made resist and working stamp materials for advancing NIL-based production technology. *Journal of Photopolymer Science and Technology, 26*, 119–124.
80. Kulmala, T. S., Rawlings, C. D., Spieser, M., Glinsner, T., Schleunitz, A., Bullerjahn, F., & Holzner, F. (2018). Single-nanometer accurate 3D nanoimprint lithography with master templates fabricated by NanoFrazor lithography. *Proceedings of SPIE, 10584*, 1058412.
81. Stevens, R., & Miyashita, T. (2010). Review of standards for microlenses and microlens arrays. *The Imaging Science Journal, 58*, 202–212.
82. Dannberg, P., Mann, G., Wagner, L., & Bräuer, A. (2000). Polymer UV-molding for micro-optical systems and O/E-integration. *Proceedings of SPIE, 4179*, 137–145.
83. Dannberg, P., Wippermann, F., Brückner, A., Matthes, A., Schreiber, P., & Bräuer, A. (2014). Wafer-level hybrid integration of complex micro-optical modules. *Micromachines, 5*, 325–340.
84. Gimkiewicz, C., Moser, M., Obi, S., Urban, C., Pedersen, J. S., Thiele, H., Zschokke, C., & Gale, M. T. (2004). Waferscale replication and testing of micro-optical components for VCSELs. *Proceedings of SPIE, 5453*, 13–26.
85. Jucius, D., Lazauskas, A., Grigaliūnas, V., Abakevičiene, B., Smetona, S., & Tamulevičius, S. (2018). UV-NIL replication of microlens arrays on flexible fluoropolymer substrates. *Microsystem Technologies, 24*, 1115–1125.
86. Senn, T., Kutz, O., Weniger, C., Li, J., Schoengen, M., Löchel, H., Wolf, J., Göttert, P., & Löchel, B. (2011). Integration of moth-eye structures into a poly(dimethylsiloxane) stamp for the replication of functionalized microlenses using UV-nanoimprint lithography. *Journal of Vacuum Science and Technology B, 29*, 061601.
87. Xie, S., Wan, X., Yang, B., Zhang, W., Wei, X., & Zhuang, S. (2019). Design and fabrication of wafer-level microlens array with moth-eye antireflective nanostructures. *Nanomaterials, 9*, 747.
88. Moharana, A. R., Außerhuber, H. M., Mitteramskogler, T., Haslinger, M. J., & Mühlberger, M. M. (2020). Multilayer nanoimprinting to create hierarchical stamp masters for nanoimprinting of optical micro- and nanostructures. *Coatings, 10*, 301.
89. Dunkel, J., Wippermann, F., Brückner, A., Reimann, A., & Bräuer, A. (2013). Fabrication of an array-like freeform molding tool for UV-replication using a step and repeat process. *Proceedings of SPIE, 8763*, 876330.
90. Brückner, A., Oberdörster, A., Dunkel, J., Reimann, A., Müller, M., & Wippermann, F. (2014). Ultra-thin wafer-level camera with 720p resolution using micro-optics. *Proceedings of SPIE, 9193*, 91930W.
91. Kim, W.-S., Lee, J.-H., Shin, S.-Y., Bae, B.-S., & Kim, Y.-C. (2004). Fabrication of ridge waveguides by UV embossing and stamping of sol-gel hybrid materials. *IEEE Photonics Technology Letters, 16*, 1888–1890.
92. Boersma, A., Wiegersma, S., Offrein, B. J., Duis, J., Delis, J., Ortsiefer, M., van Steenberge, G., Karpinen, M., van Blaaderen, A., & Corbett, B. (2013). Polymer-based optical interconnects using nanoimprint lithography. *Proceedings of SPIE, 8630*, 86300Y.
93. Hiltunen, M., Hiltunen, J., Stenberg, P., Aikio, S., Kurki, L., Vahimaa, P., & Karioja, P. (2014). Polymeric slot waveguide interferometer for sensor applications. *Optics Express, 22*, 7229–7237.
94. Hermannsson, P. G., Sørensen, K. T., Vannahme, C., Smith, C. L. C., Klein, J. J., Russew, M.-M., Grützner, G., & Kristensen, A. (2015). All-polymer photonic crystal slab sensor. *Optics Express, 23*, 16529–16539.

95. Khan, M. U., Justice, J., Petäjä, J., Korhonen, T., Boersma, A., Wiegersma, S., Karppinen, M., & Corbett, B. (2015). Multi-level single mode 2D polymer waveguide optical interconnects using nano-imprint lithography. *Optics Express, 23*, 14630–14639.
96. Zhou, C., Hedayati, M. K., & Kristensen, A. (2018). Multifunctional waveguide interferometer sensor: Simultaneous detection of refraction and absorption with size-exclusion function. *Optics Express, 26*, 24372–24383.
97. Morarescu, R., Pal, P. K., Beneitez, N. T., Missinne, J., Steenberge, G. V., Bienstman, P., & Morthier, G. (2016). Fabrication and characterization of high-optical-quality-factor hybrid polymer microring resonators operating at very near infrared wavelengths. *IEEE Photonics Journal, 8*, 6600409.
98. Cadarso, V. J., Kiefer, T., Auzelyte, V., Atasoy, H., Grützner, G., & Brugger, J. (2014). Direct imprinting of organic–inorganic hybrid materials into high aspect ratio sub-100 nm structures. *Microsystem Technologies, 20*, 1961–1966.
99. Zhu, X., Vannahme, C., Højlund-Nielsen, E., Mortensen, N. A., & Kristensen, A. (2015). Plasmonic colour laser printing. *Nature Nanotechnology, 11*, 325.
100. Calafiore, G., Koshelev, A., Allen, F. I., Dhuey, S., Sassolini, S., Wong, E., Lum, P., Munechika, K., & Cabrini, S. (2016). Nanoimprint of a 3D structure on an optical fiber for light wavefront manipulation. *Nanotechnology, 27*, 375301.
101. Koshelev, A., Calafiore, G., Piña-Hernandez, C., Allen, F. I., Dhuey, S., Sassolini, S., Wong, E., Lum, P., Munechika, K., & Cabrini, S. (2016). High refractive index Fresnel lens on a fiber fabricated by nanoimprint lithography for immersion applications. *Optics Letters, 41*, 3423–3426.
102. Calafiore, G., Koshelev, A., Darlington, T. P., Borys, N. J., Melli, M., Polyakov, A., Cantarella, G., Allen, F. I., Lum, P., Wong, E., Sassolini, S., Weber-Bargioni, A., Schuck, P. J., Cabrini, S., & Munechika, K. (2017). Campanile near-field probes fabricated by nanoimprint lithography on the facet of an optical fiber. *Scientific Reports, 7*, 1651.
103. Lorang, D. J., Tanaka, D., Spadaccini, C. M., Rose, K. A., Cherepy, N. J., & Lewis, J. A. (2011). Photocurable liquid core–fugitive shell printing of optical waveguides. *Advanced Materials, 23*, 5055–5058.
104. Neumeister, A., Himmelhuber, R., Materlik, C., Temme, T., Pape, F., Gatzen, H.-H., & Ostendorf, A. (2008). Properties of three-dimensional precision objects fabricated by using laser based micro stereo lithography. *Journal of Laser Micro/Nanoengineering, 3*, 67–72.
105. Stampfl, J., Baudis, S., Heller, C., Liska, R., Neumeister, A., Kling, R., Ostendorf, A., & Spitzbart, M. (2008). Photopolymers with tunable mechanical properties processed by laser-based high-resolution stereolithography. *Journal of Micromechanics and Microengineering, 18*, 125014.
106. Overmeyer, L., Neumeister, A., & Kling, R. (2011). Direct precision manufacturing of three-dimensional components using organically modified ceramics. *CIRP Annals, 60*, 267–270.
107. Kim, J. Y., Brauer, N. B., Fakhfouri, V., Boiko, D. L., Charbon, E., Grützner, G., & Brugger, J. (2011). Hybrid polymer microlens arrays with high numerical apertures fabricated using simple ink-jet printing technique. *Optical Materials Express, 1*, 259–269.
108. Voigt, A., Ostrzinski, U., Pfeiffer, K., Kim, J. Y., Fakhfouri, V., Brugger, J., & Grützner, G. (2011). New inks for the direct drop-on-demand fabrication of polymer lenses. *Microelectronic Engineering, 88*, 2174–2179.
109. Kim, J. Y., Pfeiffer, K., Voigt, A., Grützner, G., & Brugger, J. (2012). Directly fabricated multi-scale microlens arrays on a hydrophobic flat surface by a simple ink-jet printing technique. *Journal of Materials Chemistry, 22*, 3053–3058.
110. Grützner, G., Fink, M., Pfeiffer, K., Brugger, J., Fakhfouri, V., & Kim, J. Y. (2016). *Micro optical articles, process for their production and uses*. Patent EP2159040B1.
111. Jacot-Descombes, L., Gullo, M. R., Cadarso, V. J., & Brugger, J. (2012). Fabrication of epoxy spherical microstructures by controlled drop-on-demand inkjet printing. *Journal of Micromechanics and Microengineering, 22*, 074012.

112. Kim, J. Y., Martin-Olmos, C., Baek, N. S., & Brugger, J. (2013). Simple and easily controllable parabolic-shaped microlenses printed on polymeric mesas. *Journal of Materials Chemistry C, 1*, 2152–2157.
113. Jacot-Descombes, L., Cadarso, V. J., Schleunitz, A., Grützner, S., Klein, J. J., Brugger, J., Schift, H., & Grützner, G. (2015). Organic-inorganic-hybrid-polymer microlens arrays with tailored optical characteristics and multi-focal properties. *Optics Express, 23*, 25365–25376.
114. Wolf, J., Grützner, S., Ferstl, M., Lawal, J., Schleunitz, A., & Grützner, G. (2018). Fabrication of polymeric micro-optical components with integrated nano-topography for advanced photonic applications. In *Proceedings of the 7th GMM-Workshop: Mikro-Nano-Integration* (pp. 74–77), Dortmund: VDE Verlag.
115. Wolf, J., Grützner, S., Ferstl, M., Schleunitz, A., & Grützner, G. (2019). Assessment of additive manufacturing processes for monolithic diffractive-refractive micro-components. In *Proc. IEEE 20th International Conference on Solid-State Sensors, Actuators and Microsystems Eurosensors XXXIII* (pp. 466–469). Berlin.
116. Beckert, E., Kemper, F., Schreiber, P., Reif, M., Dannberg, P., & Sauva, S. (2019). Inkjet printing of microlens arrays on large, lithographic structured substrates. *Proceedings of SPIE, 10930*, 109300C.
117. Wachholz, P., Wolf, J., Marx, S., Weber, D., Klein, J., & Schröder, H. (2020). Novel technology for dispensing liquid polymers of a wide viscosity range on a picoliter scale for photonic applications. *Proceedings of SPIE, 11286*, 112860L.
118. Ovsianikov, A., Passinger, S., Houbertz, R., & Chichkov, B. N. (2007). Three dimensional material processing with femtosecond lasers. In C. Phipps (Ed.), *Laser ablation and its applications* (pp. 121–157). Boston, MA: Springer US.
119. Selimis, A., Mironov, V., & Farsari, M. (2015). Direct laser writing: Principles and materials for scaffold 3D printing. *Microelectronic Engineering, 132*, 83–89.
120. Multiphoton Optics GmbH. Retrieved from https://multiphoton.net/
121. Nanoscribe GmbH. Retrieved from https://www.nanoscribe.com/
122. Microlight3D. Retrieved from http://www.microlight.fr
123. Femtika. Retrieved from https://www.femtika.lt/
124. Harnisch, E., Russew, M., Klein, J., König, N., Crailsheim, H., & Schmitt, R. (2015). Optimization of hybrid polymer materials for 2PP and fabrication of individually designed hybrid microoptical elements thereof. *Optical Materials Express, 5*, 456–461.
125. Burmeister, F., Steenhusen, S., Houbertz, R., Zeitner, U. D., Nolte, S., & Tünnermann, A. (2012). Materials and technologies for fabrication of three-dimensional microstructures with sub-100 nm feature sizes by two-photon polymerization. *Journal of Laser Applications, 24*, 042014.
126. Ovsianikov, A., Shizhou, X., Farsari, M., Vamvakaki, M., Fotakis, C., & Chichkov, B. N. (2009). Shrinkage of microstructures produced by two-photon polymerization of Zr-based hybrid photosensitive materials. *Optics Express, 17*, 2143–2148.
127. Žukauskas, A., Batavičiūtė, G., Ščiuka, M., Jukna, T., Melninkaitis, A., & Malinauskas, M. (2014). Characterization of photopolymers used in laser 3D micro/nanolithography by means of laser-induced damage threshold (LIDT). *Optical Materials Express, 4*, 1601–1616.
128. Jonušauskas, L., Gailevičius, D., Mikoliūnaitė, L., Sakalauskas, D., Šakirzanovas, S., Juodkazis, S., & Malinauskas, M. (2017). Optically clear and resilient free-form μ-optics 3D-printed via ultrafast laser lithography. *Materials, 10*, 12.
129. Harnisch, E. M., & Schmitt, R. (2017). Two-photon polymerization as a structuring technology in production: Future or fiction? *Proceedings of SPIE, 10115*, 101150Q.
130. Steenhusen, S., Stichel, T., Houbertz, R., & Sextl, G. (2010). Multi-photon polymerization of inorganic-organic hybrid polymers using visible or IR ultrafast laser pulses for optical or optoelectronic devices. *Proceedings of SPIE, 7591*, 759114.
131. Perevoznik, D., Perevoznik, D., Nazir, R., Nazir, R., Kiyan, R., Kiyan, R., Kiyan, R., Kurselis, K., Koszarna, B., Gryko, D. T., Gryko, D. T., Chichkov, B. N., Chichkov, B. N., & Chichkov, B. N. (2019). High-speed two-photon polymerization 3D printing with a microchip laser at its fundamental wavelength. *Optics Express, 27*, 25119–25125.

132. Zhou, R., Malval, J.-P., Jin, M., Spangenberg, A., Pan, H., Wan, D., Morlet-Savary, F., & Knopf, S. (2019). A two-photon active chevron-shaped type I photoinitiator designed for 3D stereo-lithography. *Chemical Communications, 55*, 6233–6236.
133. Gan, Z., Cao, Y., Evans, R. A., & Gu, M. (2013). Three-dimensional deep sub-diffraction optical beam lithography with 9 nm feature size. *Nature Communications, 4*, 2061.
134. Barner-Kowollik, C., Bastmeyer, M., Blasco, E., Delaittre, G., Müller, P., Richter, B., & Wegener, M. (2017). 3D laser micro- and nanoprinting: Challenges for chemistry. *Angewandte Chemie, International Edition, 56*, 15828–15845.
135. Wollhofen, R., Buchegger, B., Eder, C., Jacak, J., Kreutzer, J., & Klar, T. A. (2017). Functional photoresists for sub-diffraction stimulated emission depletion lithography. *Optical Materials Express, 7*, 2538–2559.
136. Selimis, A., & Farsari, M. (2016). Hybrid materials for multiphoton polymerization. In J. Stampfl, R. Liska & A. Ovsianikov (Eds.), *Multiphoton lithography* (pp. 167–181). Weinheim:Wiley-VCH.
137. Malinauskas, M., Žukauskas, A., Purlys, V., Belazaras, K., Momot, A., Paipulas, D., Gadonas, R., Piskarskas, A., Gilbergs, H., Gaidukevičiūtė, A., Sakellari, I., Farsari, M., & Juodkazis, S. (2010). Femtosecond laser polymerization of hybrid/integrated micro-optical elements and their characterization. *Journal of Optics, 12*, 124010.
138. Žukauskas, A., Malinauskas, M., Reinhardt, C., Chichkov, B. N., & Gadonas, R. (2012). Closely packed hexagonal conical microlens array fabricated by direct laser photopolymerization. *Applied Optics, 51*, 4995–5003.
139. Sanchez-Padilla, B., Žukauskas, A., Aleksanyan, A., Balčytis, A., Malinauskas, M., Juodkazis, S., & Brasselet, E. (2016). Wrinkled axicons: Shaping light from cusps. *Optics Express, 24*, 24075–24082.
140. Steenhusen, S., Burmeister, F., Eckstein, H.-C., & Houbertz, R. (2015). Two-photon polymerization of hybrid polymers for applications in micro-optics. *Proceedings of SPIE, 9353*, 93530K.
141. Gissibl, T., Thiele, S., Herkommer, A., & Giessen, H. (2016). Sub-micrometer accurate free-form optics by three-dimensional printing on single-mode fibres. *Nature Communications, 7*, 11763.
142. Steenhusen, S., Hasselmann, S., & Domann, G. (2017). Strategies for rapid and reliable fabrication of microoptical structures using two-photon polymerization. *Proceedings of SPIE, 10115*, 101150S.
143. Petrov, A. K., Bessonov, V. O., Abrashitova, K. A., Kokareva, N. G., Safronov, K. R., Barannikov, A. A., Ershov, P. A., Klimova, N. B., Lyatun, I. I., Yunkin, V. A., Polikarpov, M., Snigireva, I., Fedyanin, A. A., & Snigirev, A. (2017). Polymer X-ray refractive nano-lenses fabricated by additive technology. *Optics Express, 25*, 14173–14181.
144. Johlin, E., Mann, S. A., Kasture, S., Koenderink, A. F., & Garnett, E. C. (2018). Broadband highly directive 3D nanophotonic lenses. *Nature Communications, 9*, 4742.
145. Stender, B., Hilbert, F., Dupuis, Y., Krupp, A., Mantei, W., & Houbertz, R. (2019). Manufacturing strategies for scalable high-precision 3D printing of structures from the micro to the macro range. *Advanced Optical Technologies, 8*, 225–231.
146. Brasselet, E., Malinauskas, M., Žukauskas, A., & Juodkazis, S. (2010). Photopolymerized microscopic vortex beam generators: Precise delivery of optical orbital angular momentum. *Applied Physics Letters, 97*, 211108.
147. Žukauskas, A., Malinauskas, M., & Brasselet, E. (2013). Monolithic generators of pseudo-nondiffracting optical vortex beams at the microscale. *Applied Physics Letters, 103*, 181122.
148. Woggon, T., Kleiner, T., Punke, M., & Lemmer, U. (2009). Nanostructuring of organic-inorganic hybrid materials for distributed feedback laser resonators by two-photon polymerization. *Optics Express, 17*, 2500–2507.
149. Jia, B., Serbin, J., Kim, H., Lee, B., Li, J., & Gu, M. (2007). Use of two-photon polymerization for continuous gray-level encoding of diffractive optical elements. *Applied Physics Letters, 90*, 073503.

150. Houbertz, R., Wolter, H., Schmidt, V., Kuna, L., Satzinger, V., Wüchter, C., & Langer, G. (2007). Optical waveguides embedded in PCBs—A real world application of 3D structures written by TPA. *MRS Online Proceeding Library Archive, 1054*, 1054-FF01-04.
151. Grossmann, T., Schleede, S., Hauser, M., Beck, T., Thiel, M., von Freymann, G., Mappes, T., & Kalt, H. (2011). Direct laser writing for active and passive high-Q polymer microdisks on silicon. *Optics Express, 19*, 11451–11456.
152. Siegle, T., Schierle, S., Kraemmer, S., Richter, B., Wondimu, S. F., Schuch, P., Koos, C., & Kalt, H. (2017). Photonic molecules with a tunable inter-cavity gap. *Light: Science & Applications, 6*, e16224.
153. Serbin, J., Egbert, A., Ostendorf, A., Chichkov, B. N., Houbertz, R., Domann, G., Schulz, J., Cronauer, C., Fröhlich, L., & Popall, M. (2003). Femtosecond laser-induced two-photon polymerization of inorganic–organic hybrid materials for applications in photonics. *Optics Letters, 28*, 301–303.
154. Li, J., Jia, B., & Gu, M. (2008). Engineering stop gaps of inorganic-organic polymeric 3D woodpile photonic crystals with post-thermal treatment. *Optics Express, 16*, 20073–20080.
155. Sun, Q., Juodkazis, S., Murazawa, N., Mizeikis, V., & Misawa, H. (2010). Femtosecond laser photopolymerization of photonic and free-movable microstructures in sol-gel hybrid resist. *Proceedings of SPIE, 7591*, 75910K.
156. Sakellari, I., Yin, X., Nesterov, M. L., Terzaki, K., Xomalis, A., & Farsari, M. (2017). 3D chiral plasmonic metamaterials fabricated by direct laser writing: The twisted omega particle. *Advanced Optical Materials, 5*, 1700200.
157. Gissibl, T., Thiele, S., Herkommer, A., & Giessen, H. (2016). Two-photon direct laser writing of ultracompact multi-lens objectives. *Nature Photonics, 10*, 554–560.
158. Thiele, S., Arzenbacher, K., Gissibl, T., Giessen, H., & Herkommer, A. M. (2017). 3D-printed eagle eye: Compound microlens system for foveated imaging. *Science Advances, 3*, e1602655.
159. Gailevičius, D., Padolskytė, V., Mikoliūnaitė, L., Šakirzanovas, S., Juodkazis, S., & Malinauskas, M. (2019). Additive manufacturing of 3D glass-ceramics down to nanoscale resolution. *Nanoscale Horizons, 4*, 647–651.
160. Žukauskas, A., Matulaitienė, I., Paipulas, D., Niaura, G., Malinauskas, M., & Gadonas, R. (2015). Tuning the refractive index in 3D direct laser writing lithography: Towards GRIN microoptics. *Laser & Photonics Reviews, 9*, 706–712.
161. Houbertz, R., Satzinger, V., Schmid, V., Leeb, W., & Langer, G. (2008). Optoelectronic printed circuit board: 3D structures written by two-photon absorption. *Proceedings of SPIE, 7053*, 70530B.
162. Eckel, Z. C., Zhou, C., Martin, J. H., Jacobsen, A. J., Carter, W. B., & Schaedler, T. (2016). Additive manufacturing of polymer-derived ceramics. *Science, 351*, 58–62.
163. Zanchetta, E., Cattaldo, M., Franchin, G., Schwentenwein, M., Homa, J., Brusatin, G., & Colombo, P. (2016). Stereolithography of SiOC ceramic microcomponents. *Advanced Materials, 28*, 370–376.
164. Marino, A., Ciofani, G., Filippeschi, C., Pellegrino, M., Pellegrini, M., Orsini, P., Pasqualetti, M., Mattoli, V., & Mazzolai, B. (2013). Two-photon polymerization of sub-micrometric patterned surfaces: "Investigation of cell-substrate interactions and improved differentiation of neuron-like cells". *ACS Applied Materials & Interfaces, 5*, 13012–13021.
165. Marino, A., Filippeschi, C., Genchi, G. G., Mattoli, V., Mazzolai, B., & Ciofani, G. (2014). The Osteoprint: A bioinspired two-photon polymerized 3-D structure for the enhancement of bone-like cell differentiation. *Acta Biomaterialia, 10*, 4304–4313.
166. Turunen, S., Joki, T., Hiltunen, M. L., Ihalainen, T. O., Narkilahti, S., & Kellomäki, M. (2017). Direct laser writing of tubular microtowers for 3D culture of human pluripotent stem cell-derived neuronal cells. *ACS Applied Materials & Interfaces, 9*, 25717–25730.
167. Buchroithner, B., Hartmann, D., Mayr, S., Oh, Y. J., Sivun, D., Karner, A., Buchegger, B., Griesser, T., Hinterdorfer, P., Klar, T. A., & Jacak, J. (2020). 3D multiphoton lithography using bio-compatible polymers with specific mechanical properties. *Nanoscale Advances, 2*, 2422–2428.

168. Klein, F., Richter, B., Striebel, T., Franz, C. M., von Freymann, G., Wegener, M., & Bastmeyer, M. (2011). Two-component polymer scaffolds for controlled three-dimensional cell culture. *Advanced Materials, 23*, 1341–1345.
169. Rekštyte, S., Kaziulionyte, E., Balciunas, E., Kaškelyte, D., & Malinauskas, M. (2014). Direct laser fabrication of composite material 3D microstructured scaffolds. *Journal of Laser Micro/Nanoengineering, 9*, 25–30.
170. Qiu, F., Zhang, L., Peyer, K. E., Casarosa, M., Franco-Obregón, A., Choi, H., & Nelson, B. J. (2013). Noncytotoxic artificial bacterial flagella fabricated from biocompatible ORMOCOMP and iron coating. *Journal of Materials Chemistry B, 2*, 357–362.
171. Gao, Z., Li, H., Chen, X., & Zhang, H. P. (2015). Using confined bacteria as building blocks to generate fluid flow. *Lab on a Chip, 15*, 4555–4562.
172. Bertin, N., Spelman, T. A., Combriat, T., Hue, H., Stéphan, O., Lauga, E., & Marmottant, P. (2017). Bubble-based acoustic micropropulsors: Active surfaces and mixers. *Lab on a Chip, 17*, 1515–1528.
173. Plamadeala, C., Gosain, S. R., Hischen, F., Buchroithner, B., Puthukodan, S., Jacak, J., Bocchino, A., Whelan, D., O'Mahony, C., Baumgartner, W., & Heitz, J. (2020). Bio-inspired microneedle design for efficient drug/vaccine coating. *Biomedical Microdevices, 22*, 8.
174. Stocker, M. P., Li, L., Gattass, R. R., & Fourkas, J. T. (2011). Multiphoton photoresists giving nanoscale resolution that is inversely dependent on exposure time. *Nature Chemistry, 3*, 223–227.
175. Tumbleston, J. R., Shirvanyants, D., Ermoshkin, N., Janusziewicz, R., Johnson, A. R., Kelly, D., Chen, K., Pinschmidt, R., Rolland, J. P., Ermoshkin, A., Samulski, E. T., & DeSimone, J. M. (2015). Continuous liquid interface production of 3D objects. *Science, 347*, 1349–1352.
176. de Beer, M. P., van der Laan, H. L., Cole, M. A., Whelan, R. J., Burns, M. A., & Scott, T. F. (2019). Rapid, continuous additive manufacturing by volumetric polymerization inhibition patterning. *Science Advances, 5*, eaau8723.
177. Dolinski, N. D., Page, Z. A., Callaway, E. B., Eisenreich, F., Garcia, R. V., Chavez, R., Bothman, D. P., Hecht, S., Zok, F. W., & Hawker, C. J. (2018). Solution mask liquid lithography (SMaLL) for one-step, multimaterial 3D printing. *Advanced Materials, 30*, 1800364.
178. Gernhardt, M., Blasco, E., Hippler, M., Blinco, J., Bastmeyer, M., Wegener, M., Frisch, H., & Barner-Kowollik, C. (2019). Tailoring the mechanical properties of 3D microstructures using visible light post-manufacturing. *Advanced Materials, 31*, 1901269.
179. del Barrio, J., & Sánchez-Somolinos, C. (2019). Light to shape the future: From photolithography to 4D printing. *Advanced Optical Materials, 7*, 1900598.
180. Hippler, M., Blasco, E., Qu, J., Tanaka, M., Barner-Kowollik, C., Wegener, M., & Bastmeyer, M. (2019). Controlling the shape of 3D microstructures by temperature and light. *Nature Communications, 10*, 232.